Åbo Akademi

Dimitar Valtakari

Printed and Coated Functionality on Natural Fibre-Based Substrates

Laboratory of Paper Coating and Converting
Centre for Functional Materials at Biological Interfaces
Faculty of Science and Engineering

Dimitar Valtakari

Born 1970 in Turku, Finland.

MSc in Physical Chemistry, Åbo Akademi University, Finland in 2008

Printed and Coated Functionality on Natural Fibre-Based Substrates

Dimitar Valtakari

Laboratory of Paper Coating and Converting
Centre for Functional Materials at Biological Interfaces (FunMat)
Faculty of Science and Engineering
Åbo Akademi University
Åbo/Turku, Finland
2018

Supervisor

Adjunct Professor Jarkko J. Saarinen
Åbo Akademi University, Turku, Finland

Professor Martti Toivakka
Åbo Akademi University, Turku, Finland

Pre-examiners

Professor Magnus Lestelius
Department of Engineering and Chemical Sciences
Karlstads Universitet, Karlstad, Sweden

and

Professor Toshiharu Enomae
Laboratory of Paper Device and Eco-friendly Material Sciences
Department of Appropriate Technology and Sciences for Sustainable Development
University of Tsukuba, Tsukuba, Ibaraki, Japan

Opponent for the public defence

Professor Magnus Lestelius
Department of Engineering and Chemical Sciences
Karlstads Universitet, Karlstad, Sweden

ISBN 978-952-12-3651-8 (print)
ISBN 978-952-12-3652-5 (digital)
Painosalama Oy, Turku, Finland, 2018

If the music make you move
'Cause you can dig the groove
Then groove on, groove on
If you feel like you wanna make love
Under the stars above
Love on, love on
If there's something you wanna say
And talkin' is the only way
Rap on, oh, rap on
'Cause whatever, oh, you do
Oh, you've got to do your thing

~

If you feel like you wanna scream
'Cause that's your way of lettin' off steam
Scream on, scream on
If you feel like you wanna sing
'Cause singing is your thing
Sing on, sing on
If you wanna make love all night
And you feel it's right
Right on, right on
Cause whatever, oh, you do
Oh, you've got to do your thing
Do your thing …

"Do Your Thing" by Isaac Hayes (1971)

Foreword and Acknowledgments

This thesis work has been carried out at the Laboratory of Paper Coating and Converting between 2011 and 2016 within the framework of the Centre for Functional Materials (FunMat, 2011-13), a National Centre of Excellence appointed by the Academy of Finland. All research was conducted on fulltime basis funded by the Academy of Finland (grant nos. 250 122, 256 263, and 283 054).

I wish to thank my primary supervisor Docent Jarkko J. Saarinen for his phenomenal insight and relentless support in bringing this doctoral thesis to its final stage. Prof. Martti Toivakka is also greatly acknowledged for his input in the process. The staff, colleagues, past and present room-mates (Manuela, Milena, Daniela and Vinay), turned this chapter of my life into a most memorable experience. Thank you, all for being part of it!

A great deal of time was spent at the physics lab preparing and measuring samples. I am grateful to Prof. Ronald Österbacka, Dr Fredrik Petterson, and Dr Kjell-Mikael Källman for letting me use their lab facilities and equipment, and helping me out in various situations.

On a personal level, the pursuit for the PhD degree commenced a few years earlier, in April 2009. Prof. Jouko Peltonen, Dr Petri Ihalainen, and Dr Anni Määttänen, core members of the research group at the time, are greatly acknowledged for introducing me to the world of printed electronics, and printed functionality.

April 2017,

Dimitar Valtakari

List of Publications

List of Included Publications

I. *Flexographic printing of PEDOT:PSS on coated papers for printed functionality,* D. Valtakari, R. Bollström, M. Tuominen, H. Teisala, M. Aromaa, M. Toivakka, J. Kuusipalo, J.M. Mäkelä, J. Uozumi and J.J. Saarinen, Journal of Print and Media Technology Research, **2**, 7-13 (2013)

II. *Influence of anionic and cationic polyelectrolytes on the conductivity and morphology of poly(3-,4-ethylenedioxythiophene):poly(styrene-sulfonate) films*, D. Valtakari, R. Bollström, M. Toivakka and J.J. Saarinen, Thin Solid Films, **590**, 170-176 (2015)

III. *Conductivity of PEDOT:PSS on spin coated and drop cast nanofibrillar cellulose thin films*, D. Valtakari, J. Liu, V. Kumar, C. Xu, M. Toivakka and J.J. Saarinen, Nanoscale Research Letters, **10**, 386 (2015)

IV. *Planar fluidic channels on TiO_2 nanoparticle coated paperboard,* D. Valtakari, M. Stepien, J. Haapanen, H. Teisala, M. Tuominen, J. Kuusipalo, J.M. Mäkelä, M. Toivakka, J.J. Saarinen, Nordic Pulp & Paper Research Journal, **31**, 232-238 (2016)

List of Supporting Publications

Articles in Peer-reviewed International Journals

S1. *Paper-based planar reaction arrays for printed diagnostics,* A. Määttänen, D. Fors, S. Wang, D. Valtakari, P. Ihalainen, and J. Peltonen, Sensors and Actuators B: Chemical, **160**, 1404-1412 (2011)

S2. *Surface-enhanced Raman scattering active substrates by liquid flame spray deposited and inkjet printed silver nanoparticles,* J.J. Saarinen, D. Valtakari, J. Haapanen, T. Salminen, J.M. Mäkelä, and J. Uozumi, Optical Review, **21**, 339-344 (2014)

S3. *Composite films of nanofibrillated cellulose and o-acetyl galactoglucomannan (GGM) coated with succinic esters of GGM showing potential as barrier material in food packaging*, Kisonen, K. Prakobna, C. Xu, A. Salminen, K.S. Mikkonen, D. Valtakari, P. Eklund, J. Seppälä, M. Tenkanen, and S. Willför, Journal of Material Science, **50**, 3189-3199 (2015)

S4. *Roll-to-roll manufacturing of disposable surface-enhanced Raman scattering (SERS) sensors on paper based substrates,* J.J. Saarinen, D. Valtakari, S. Sandén, J. Haapanen, T. Salminen, J.M. Mäkelä, and J. Uozumi, Nordic Pulp & Paper Research Journal, **32**, 222-228 (2017).

International Peer-reviewed Conference Papers

C1. *Conductive surfaces on coated papers by flexographic printing,* D. Valtakari, R. Bollström, M. Tuominen, H. Teisala, M. Aromaa, M. Toivakka, J. Kuusipalo, J.M. Mäkelä, J. Uozumi and J.J. Saarinen, 12th TAPPI Advanced Coating Fundamentals Symposium, Atlanta, GA, USA, September 10-12, 2012. Atlanta, GA: TAPPI Press (2012)

C2. *Effect of polyelectrolytes on conductivity for printed functionality,* D. Valtakari, R. Bollström, M. Toivakka, J.J. Saarinen, 41st Inter-national Research Conference of International Association of Research Organizations for the Information, Media and Graphic Arts Industries (iarigai), Swansea, UK, September 7-10, 2014. Advances in Printing and Media Technology: Proceedings of the 41st International Research Conference of iarigai, Darmstadt, DE (2014)

Author's Contribution

Publication I The author performed together with the co-authors the experimental work and data analysis of the experimental results. The author wrote the first draft of the article. The liquid flame spray TiO_2 nanoparticle coated paperboard was fabricated by the Tampere University of Technology.

Publication II The author was responsible for planning the experimental work. The author conducted all the experiments and carried out data analysis of the experimental data. The author wrote the article.

Publication III The author was responsible for planning the experimental work. The author conducted all the experiments and carried out data analysis of the experimental data. Nanofibrillar cellulose was produced and characterized by M.Sc. Jun Liu (Åbo Akademi University, Turku, Finland). The author wrote the article.

Publication IV The author took a part in planning the experimental work and carried out the sample preparation. The liquid flame spray TiO_2 nanoparticle coated paperboard was fabricated by the Tampere University of Technology. SEM, XPS, and ToF-SIMS surface characterization and data analysis was performed by PhD Milena Stepien.

Abstract

Mass-produced, paper-based printed electronics can provide a solution for the manufacturing of flexible and disposable electronic applications of the future. Traditional recyclable, high throughput, and low-cost roll-to-roll paper coating and printing processes were originally designed around conventional paper, graphics and packaging industry. Control over surface wetting properties is essential for several paper-related processes such as printing, coating and laminating. Good control over wettability, i.e. control over surface chemistry and structure, creates new possibilities for surface engineering. In this respect, printed functionality sets specific requirements on paper substrates and functional inks. This requires fundamental understanding of how to modify the surface chemistry and structure of the specialty paper qualities and the corresponding functionalized inks.

In this work, the effect of surface modification on ink transfer and consecutively, electrical conductivity of the water-based conductive polymer ink PEDOT:PSS was studied. Conventional PEDOT:PSS is applied on a transparent surface such as glass or plastic film. In **Paper I**, the PEDOT:PSS was printed using flexography on a TiO_2 liquid flame spray (LFS) nanoparticle coated paperboard. The wetting behaviour of the TiO_2 nanoparticle treated surface can be controlled between highly hydrophilic and superhydrophobic states when exposed to UV-light or thermal energy, respectively. The LFS nanoparticle deposition method is also compatible with the roll-to-roll process flow typically applied in paper and paperboard production.

Paper coating is the most common way to adjust the paper or paperboard surface properties. As such, the coating layer is the first component to interact with functional inks. The mineral pigment particles used in the coating formulations are typically covered by polyelectrolytes. Therefore, enhancement or adverse effects from the interaction between PEDOT:PSS and polyelectrolytes was studied in **Paper II**. The polyelectrolyte concentrations in paper coatings and especially on pigment particle surfaces tend to be fairly low and, therefore, difficult to reproduce under controlled laboratory conditions. At higher concentrations, the conductivity of PEDOT:PSS was greatly enhanced by the presence of an oppositely charged cationic electrolyte. The mechanism is identical to the one caused between oppositely attracted species in the layer-by-layer deposition technique.

The interaction between two adjacent, tuneable layers had been limited to wetting differences or attraction of opposite species. Introducing PEDOT:PSS on top of nanofibrillated cellulose (NFC) mixed with glycerol, which are both active functional materials, provided additional alternative approaches, as shown in **Paper III**. By altering the coating structure, the NFC can be converted into a barrier layer which, however, does not provide additional conductivity enhancement to PEDOT:PSS. NFC can also be used as a reservoir layer designed to release constituents into the PEDOT:PSS layer leading to a conductivity improvement. The NFC barrier and reservoir layer approaches provide possibilities for organic thin film electronics applications, both as stand-alone and/or stacked configurations.

Finally, in **Paper IV** a new design for permanent, low-cost, and planar fluidic channels on LFS TiO_2 nanoparticle coated paperboard (introduced in **Paper I**) was demonstrated. The reversible wettability characteristics of the TiO_2 nanoparticle layer was made permanent by using a wetting step after the first stage UV irradiation. Hereby, the LFS deposited TiO_2 nanoparticles are partially removed from the surface forming a permanent channel. The approach can provide avenues for disposable and biodegradable point-of-care diagnostics based on planar fluidic channels.

Keywords

Printed functionality, printed electronics, paper electronics, wetting, sustainable development, PEDOT:PSS, polyelectrolyte, nanofibrillar cellulose (NFC), thin films, TiO_2, liquid flame spray (LFS), nanoparticle, fluidic channel.

Svensk Sammanfattning

Masstillverkad tryckt elektronik på papper kan erbjuda en lösning för framställningen av framtida flexibla elektroniska engångsartiklar. Traditionella pappersbestrycknings- och tryckprocesser kännetecknas av återvinning, hög produktionskapacitet och kontinuerliga rullbaserade lågkostnads tillverkningsmetoder, som en gång i tiden skapades för att bemöta den konventionella pappers-, grafiska, och förpackningsindustrins krav. Kontroll över ytans vätningsegenskaper har avgörande betydelse i flera pappersrelaterade processer som tryckning, bestrykning och laminering. God kontroll över vätning, dvs. kontroll över ytans kemi och struktur, kan skapa nya möjligheter för tekniskt avancerad framställning av ytor. Tryckt funktionalitet och smarta egenskaper ställer i detta avseende särskilda krav på huruvida och i vilken grad ytkemin och bestrykningsskiktets struktur hos papperssubstrat bör kunna modifieras samt tryckfärger funktionaliseras.

I detta arbete studerades ytmodifieringens inverkan på överföringen av den vattenbaserade polymeren/tryckfärgen PEDOT: PSS och dess elektriska ledningsförmåga. Konventionell PEDOT: PSS appliceras på en genomskinlig yta som glas eller plastfilm. I **Publikation I** flexotrycktes PEDOT: PSS på TiO2 -nanopartikel vätskeflambesprutad (LFS) kartong. TiO2 – behandlade ytans vätningsegenskaper kan producera omställbara superhydrofila och superhydrofoba vätningstillstånd då denna utsätts för UV-ljus respektive värmebehandling. LFS-metoden är förenlig med kontinuerliga pappers- och kartongtillverkningens rullbaserade tillverkningsprocesser.

Ytegenskaperna hos papper och kartong justeras vanligtvis med bestrykningsskikt. Det är således bestrykningsskiktet som i första hand som kommer i kontakt och växelverkar med funktionella tryckfärger. Mineralpigmentpartiklarna i bestrykningssmeten är typiskt täckta med polyelektrolyter. Förbättringar eller negativa konsekvenser till följd av växelverkan mellan PEDOT:PSS och polyelektrolyter studerades i **Publikation II**. Pappersbestrykningar och speciellt pigmentpartikelytor tenderar mot låga polyelektrolythalter som är svåra att reproducera under kontrollerade laboratoriebetingelser. PEDOT:PSS ledningsförmåga förbättrades markant i närvaro av högre halter av motsatt laddade katjoniska elektrolyter. Mekanismen är identisk med denna i layer-by-layer -ytbeläggningsmetoden där ett nytt skikt bildas som resultat av attraktion mellan motsatt laddade arter. Växelverkan mellan två intilliggande, justerbara skikt hade hittills begränsats till vätnings- eller attraktionsskillnader. **Publikation III** demonstrerar

appliceringen av PEDOT:PSS ovanpå nanofibrillerad cellulosa (NFC) med glycerol, där båda utgör aktiva funktionella material, och tillhandahåller flera alternativa strategier. Genom att justera NFC's bestrykningsstruktur kan detta konverteras till ett barriärskikt utan någon vidare bidrag till förbättring av ledningsförmågan hos PEDOT: PSS. NFC kan också bistå som ett reservoarskikt som har som uppgift att frigöra glycerol och vatten i in PEDOT: PSS -skiktet och därpå följande utökning av elektrisk konduktivitet. Barriär- och reservoaregenskaperna hos NFC kan bana väg för organiska applikationer för tunnfilmsbaserad elektronik, både som fristående och/eller på varandra staplade konfigurationer.

Arbetet avrundades med att i **Publikation IV** demonstrera en nydesignad billig tvådimensionell flödeskanal av bestående karaktär på TiO2-nanopartikel vätskeflambesprutad (LFS) kartong (presenterad i **Publikation I**). Det reversibelt omställbara TiO2-nanoskiktets vätningstillstånd låstes genom ett första stegs UV-bestrålning och vätning. TiO2-nanopartiklarna röjs delvis från ytan under processens gång vilket blottlägger en bestående kanal. Tillvägagångssättet kan bana väg för nedbrytbara diagnostiska engångsartiklar som baserar sig på tvådimensionella flödeskanaler.

Nyckelord

Tryckt funktionalitet, tryckt elektronik, papperselektronik, vätning, hållbar utveckling, PEDOT:PSS, polyelektrolyt, nanocellulosa (NFC), tunna filmer, TiO2, vätskeflambesprutning (LFS), nanopartiklar, (mikro)flödeskanaler.

Abbreviations and Nomenclature

Abbreviations

ALD	atomic layer deposition
CA	contact angle
CVD	chemical vapour deposition
LFS	liquid flame spray
MLCP	multilayer coated paper
NFC	nanofibrillar cellulose
NFC-G	nanofibrillar cellulose/glycerol mixture
PA	sodium polyacrylate
pDADMAC	poly(dimethyldiallylammonium chloride)
PEDOT:PSS	poly(ethylelene-dioxythiophene):polystyrene sulfonate
PET	poly(ethylene terephthalate)
PVD	physical vapour deposition
SEM	scanning electron microscopy
ToF-SIMS	time-of-flight secondary ion mass spectrometry
UV	ultraviolet radiation
UVA	ultraviolet A radiation
WCA	water contact angle
XPS	X-ray photoelectron spectroscopy

Nomenclature

γ	[mN/m]	interfacial (surface) tension
θ	[°]	contact angle (theta)
R	[Ω cm]	resistivity
$R_{\square}$	[Ω/□]	sheet resistance

Contents

Chapter 1

Introduction

Since the beginning of the 21st century, printed electronics and printed intelligence have attracted a growing interest with market value forecasts up to 45 billion USD by 2022 (Das & Zerros 2012). Printed electronics have typically been manufactured on plastics and glass. Plastic substrates provide significant flexibility, and thus roll-to-roll scalability for printed and coated flexible electronics. Such printed electronics can be used in a broad variety of light-weight, disposable applications ranging from intelligent packaging, solar panels, radio frequency identification (RFID) tags to medical implants, wearable computers, and various sensors. Moreover, internet of things (IoT) is a growing megatrend that will utilize printed, thin electronic structures on flexible substrates. To reduce the environmental burden of electronic waste recyclability becomes an important factor (Irimia-Vladu et al. 2012). This has resulted in the search for more ecologically and economically sustainable substrates that are both cost-effective and widely available. Renewable, recyclable, and biodegradable natural fibre-based substrates such as paper and paperboard are currently produced annually in millions of tons, but mostly they are used for the needs of the conventional graphical arts and packaging industry.

A limited market growth and at the same time rising production costs have led the forest products industry to search for expansion of the conventional product portfolio towards value-added functionalities on natural fibre-based products such as functional packages and paper-based sensor applications. Natural fibre-based substrates serve as environmentally and ecologically sustainable substitutes for plastic and glass. Cellulose is the most abundant biopolymer on the Earth and thus a suitable candidate for replacing fossil fuel-based solutions with sustainable and cost-effective alternatives. Paper can be 1000 times less expensive than glass substrates and 100 times less expensive than plastic films (Tobjörk & Österbacka 2011). However, the intrinsic properties of paper, such as porosity and surface roughness, need to be taken into account for printed electronics. Conventional technologies developed for graphical arts applications improving the paper appearance and print quality such as mineral pigment coating, calendering, and barrier layers can also be used to tailor both porosity and surface roughness for printed functionality applications.

Printed and coated functionality on natural fibre-based substrates is not only restricted to paper-based electronics (Tobjörk & Österbacka 2011) such as transistors (Bollström et al. 2009), displays (Siegel et al. 2009), and photovoltaics (Barr et al. 2011, Hübler et al. 2011). Bioactive paper for low-cost diagnostics (Pelton 2009), gas sensors (Sarfraz et al. 2012) and microfluidic devices on paper (Martinez et al. 2008, Martinez et al. 2010, Fobel et al. 2014, Songok et al. 2014) have been demonstrated.

The present work deals with fundamentals of functional surface modification of natural fibre-based substrates ranging from paper and paperboard to nanocellulose films. The overall objective was to understand the physico-chemical interactions arising from the chosen functional surface modifications and their influence on the functional performance. Specific targets aimed at (i) understanding the printability and behaviour of a conductive polymer (PEDOT:PSS) on the various substrates, (ii) clarifying the interactions between PEDOT:PSS and polyelectrolytes commonly used in papermaking, and (iii) demonstrating controlled wettability of coated paper for controlling functional printability or microfluidic flow.

Printed and coated electronics, including controlled wetting, were investigated together with TiO_2 nanoparticle surface functionalization. In **Paper I** the effect of coating structure and surface wettability on large area conductive surfaces was studied on various coated paper grades, including a liquid flame spray (LFS) functionalized TiO_2 nanoparticle coated paperboard with controlled wettability from superhydrophobic to highly hydrophilic state. Surface wettability has an effect on printability with water-based conductive inks such as poly(3,4-ethylenedioxythiophene): poly(styrenesulfonate) (PEDOT:PSS). **Paper II** focuses on aspects related to the surface conductive paper electronics typically fabricated on coated paper grades (Denneulin et al. 2008, Bollström et al. 2009, Trnovek et al. 2009, Amin et al. 2012), and the effect of both cationic and anionic polyelectrolytes on conductivity of PEDOT:PSS. Such polyelectrolytes are typically used during the papermaking and are thus present on the surface of natural fibre-based substrates. **Paper III** investigates the interaction between spin-coated and drop cast nanofibrillar (NFC) thin films mixed with glycerol and conductivity of subsequent PEDOT:PSS application. Finally, in **Paper IV** a permanent planar fluidic channel was demonstrated on the LFS TiO_2 nanoparticle coated paperboard. The reversible wettability transition can be made permanent by a first stage wetting, i.e. the UV irradiated channel area is exposed to water that will partially remove the deposited TiO_2 nanoparticles, and a permanent channel is formed.

Natural fibre-based substrates have potential in many applications outside the conventional graphic arts industry promoting sustainable transformation from fossil fuel-based plastic substrates to renewable natural fibre-based platforms for printed electronics, photonics, and intelligence applications in the future.

Chapter 2

Background

Cellulose is the most abundant natural biopolymer on Earth with annual production up to 1.8×10^{12} tons (Eveleigh 1987). Traditionally, cellulose fibres have been used in different paper products, from newspapers, magazines, and packaging applications to paperboard boxes and wrapping papers. However, with the growth of the electronic and social media, consumption of traditional paper grades has decreased in the developed countries. Hence, functional applications with added value on paper-based substrates have raised interest as they potentially provide both economically and ecologically sustainable alternatives for fossil fuel-based plastic substrates.

2.1 Functional printing and functional paper products

Flexographic printing has traditionally been utilized in the packaging industry for a wide range of flexible and non-flexible substrates with high throughput (Kuusipalo 2008). For printed electronics applications, printing can be used to scale up from laboratory scale batch processes to mass printing volumes. The advantage of printing compared to coating methods is the possibility for patterning (Tobjörk et al. 2008). The added complexity defined by the device structures in electronics typically involves multilayer structures only achievable through several successive printing or coating steps or a combination of these. The lack of orthogonal solvents, i.e. solvents not dissolving the previously printed layer, can limit the number of successive print layers. Current hybrid printers commonly combine state-of-the-art roll-to-roll (R2R) demonstrators utilizing a slot die coater, and gravure, inkjet, or flexographic printing units.

Common techniques used in printed electronics comprise screen, inkjet, and flexographic printing (Tobjörk & Österbacka 2011). They are typically used for conductive patterns and circuits on various substrates ranging from rigid (glass, silicon) to flexible (plastic, paper, nanocellulose films) alternatives. R2R processes provide a route for cost-effective manufacturing of organic electronic devices, i.e. an all-in-line printing process allows a significant unit cost reduction of the printed devices (Berggren et al. 2007).

Printed and coated functionality on natural fibre-based substrates covers various approaches from electronics and energy applications to diagnostic

devices and sensors. These include transistors (Bollström et al. 2009), displays (Siegel et al. 2009), light-emitting paper (Asadpoordarvish et al. 2015), electric paper actuators (Hamedi et al. 2016) and photovoltaic demonstrators (Barr et al. 2011, Hübler et al. 2011), as well as bioactive paper for low-cost diagnostics (Pelton 2009), gas sensors (Sarfraz et al. 2012), a low-cost platform for electrochemical analysis (Määttänen et al. 2013) and microfluidic devices on paper (Martinez et al. 2008, Martinez et al. 2010, Dungchai et al. 2009, Nie et al. 2010, Fobel et al. 2014, Songok et al. 2014, Valtakari et al. 2016).

2.2 Paper electronics and conductivity

Paper-based electronics is typically based on either bulk or surface conductivity. In bulk conductivity, the entire paper is functionalized to become an electrically conductive integral device component. This can be achieved, for example, by immersing or coating an uncoated paper with conductive polymers, or by in-situ polymerization in the paper (Björklund & Lundström 1984, Huang et al. 2006, Qian et al. 2006, Montibon et al. 2010). Bulk conductivity can also be achieved directly from wood pulp fibres that are coated by a multi-sequenced, layer-by-layer method with conductive polymers or particles (Agarwal et al. 2006, Zheng et al. 2006, Wistrand et al. 2007, Peng et al. 2008). Alternatively, adding silver plated carbon fibres or mixing of metalized polyester fibres provides alternative routes for conductive paper production (Shinagawa et al. 1999, Jang & Ryu 2006).

In the surface conductivity category, besides printing simple conductive non-patterned or patterned areas on paper (Mäkelä et al. 2003, Tobjörk & Österbacka 2011), an increasing number of devices and concepts have been demonstrated, such as an all-organic active matrix display (Andersson et al. 2003), a passive ultra-high radio frequency identification tag module embedded in a paper-on-paper structure (Yang et al. 2007), moisture and temperature sensors (Unander & Nilsson 2009, Courbat et al. 2011), an ethanol sensor (Arena et al. 2010), and a piezoresistive microelectromechanical force sensor (Liu et al. 2011).

Functional materials on a paper substrate can be designated for a singular purpose. However, the functional materials placed on the paper surface cover a wide range from simple single layer conductive coatings or patterns to complex stacked structures with each layer fulfilling a specific purpose (Cui 2016). Simple electronics incorporate structures that fall into the following categories according to their electrical properties: conductor, semiconductor,

insulator, or dielectric (Bao 2000). On the paper surface, specific electrical characteristics of single stacked layers are achieved by sequential printing or coating steps using either organic or inorganic functional materials. In terms of conductivity, inorganic materials provide a higher conductivity but with limited flexibility (He et al. 2015). Typical printable inorganic materials on paper are metals such as silver, copper, gold, and aluminium (Perelaer et al. 2010). Carbon allotropes typically employed in printed organic electronics range from small molecule fullerenes and carbon nanotubes (CNT's) to large molecule graphite minerals (crystalline carbon and semi-metal) and graphene with plenty of customization options that can vary from being semi-conductive to conductive (Jariwala et al. 2013). The used particle size of metal inks depends on the printing method, ranging from micron-sized flakes in the more viscous flexographic and screen printing inks mainly for thick ink layers (0.8-100 μm) and low resolution (20-100 μm) to nanoparticles in low-viscous inkjet inks for thin ink layers (0.3-20 μm) and fine resolution (20-50 μm) (Nelo 2016). Large particle size metal inks are more suitable for rougher substrate surfaces while being less sensitive to surface-related imperfections and defects. Until recently, metal nanoparticle inks required a high temperature sintering for printed structures to become conductive (Magdassi 2009). The sintering step has two functions: to remove the organic protective layers covering the nanoparticles to prevent aggregation in the ink dispersion, and to initiate necking, i.e. allowing the discrete metal nanoparticles melt partially forming a continuous film or matrix network, for better conductivity. This created new problems, as the substrate needs to withstand high sintering temperatures (Laakso et al. 2009). The sintered metal structure placed on top of a stacked electronic structure can also cut through the underlying organic layers. Alternative strategies have been applied to solve this issue that approached the problem from two different directions: by developing more selective sintering methods, e.g. scanned laser irradiation, absorption of microwave radiation, low pressure argon plasma, UV radiation, photonic flash sintering (UVA to NIR), high temperature plasma, or electrical current sintering that results in less harm to the surrounding materials (Cui 2016). Alternatively, more sophisticated metal inks have been developed that become conductive at much lower temperatures (Cui 2016). In the former approach, sintering takes place locally and for a limited period of time, being suitable for most substrate types and allowing the use of nanoparticle inks with otherwise limited sintering properties. However, this approach may require very specific and often expensive sintering units (Cui 2016) contrary to the conventional thermal curing sources. Hence, low-

temperature sintering inks have gained more interest since the pioneering work by Mitsubishi (Yoshiki et al. 2007). These inks are typically based on metal-salt formulations (Perelaer & Schubert 2013) that become conductive by chemical metallization at the substrate surface. The activating substance can be added simultaneously during printing or it can be added directly in the specialty paper substrate coating.

Organic functional materials are preferred, as they enable a liquid phase processing and material flexibility similar to the conventional printing inks (Sekine et al. 2014). Thus, they fill all the requirements for a roll-to-roll, high volume processing. Ecological as well as health hazard considerations to minimize the evaporation of organic solvents into the environment have triggered a transition from solvent-based inks towards water-based inks (Izdebska & Thomas 2016). On plastic substrate, high surface tension of water may cause wetting problems at ink setting and lowered adhesion of dried ink. Paper, however, provides a substrate platform with fully adjustable surface energy. Under clean room conditions, dust residues originating from the paper substrate may act as a source of operational hazard in printed electronics. The absence of organic solvent vapours could turn paper into the optimal substrate for printing at ambient conditions.

Polyaniline (PANI), polythiophenes, and polypyrroles are typical conductive polymer groups (Wang et al. 1990). Among the polythiophenes, poly(3,4-ethylene-dioxythiophene) polystyrene sulfonate or PEDOT:PSS has so far reached the most widespread popularity: partly due to its non-solvent-based and user-friendly handling, and partly due to the numerous options for fine tuning the polymer complex to meet either conductor/semiconductor material specifications or more specific printing method requirements.

Thiophene polymers designed especially for semiconductor use are poly(3-hexylthiophene-2,5-diyl) regioregular (P3HT) (Padinger et al. 2003, Li et al. 2005), poly(3,3'''-didodecylquaterthiophene) (PQT-12) (Arias et al. 2004), and poly(2,5–bis(3-tetradecylthiophen-2-yl)thieno[3,2-b]thiophene (pBTTT-C14) (McCulloch et al. 2006). From a high performance and stability point of view, a good quality semiconductor/dielectric interface is essential in printed electronics. Organic dielectrics dissolve more easily in solvents and solutions than their inorganic counterparts, resulting in a better overall print quality. Commonly used printed electronics organic insulators and dielectric materials comprise polymers such as polystyrene, polyvinyl alcohol, polyimide, polyethylene terephthalate, and poly (4-vinylphenol) (Søndergaard et al. 2013, Khan et al. S 2015). Printed electronic components that use insulator and

dielectric parts include transistors, capacitors, and protecting conductive layers and wiring from short circuits. Solution-processed printability makes these organic dielectrics also suitable for final encapsulation material of the printed devices. Beside basic categorization based on the degree of electrical conductivity, some materials can also provide luminescence and electrochromic or selective gas or liquid phase sensing properties (Tekin et al. 2005, Möller et al. 2010, Mattana & Briand 2016).

Surface roughness and porosity of paper are very different compared to plastic film or glass substrates. For printed electronics, these characteristics of the paper substrate play an important role, for example, for electrical conductivity of printed or coated conductive layers. In general, a higher surface roughness in the short length scale (0.4-1.2 μm) will decrease the conductivity (Ihalainen et al. 2012). Lamination of a plastic film on the paper surface can be used to avoid the problems with porosity or surface roughness. However, a more sustainable solution is to use only cellulose-based structures, and therefore, much effort has been dedicated to finding suitable coating concepts for paper in printed electronics.

Conductivity of a printed pattern depends on both surface and the ink properties. In general, thick and high viscous inks are less sensitive to paper surface characteristics as they form thicker and coarser patterns at the substrate. The downside of such inks is that very fine printed structures are difficult to achieve. The consumption of the conductive material is also high. The amount of resins and thickeners in the ink composition is considerable, thus making it difficult to remove. Alternatively, low-viscosity inks produce thinner and finer conductive patterns. These inks are heavily absorbed by the paper substrate that results in a weaker conductivity unless the paper properties are selected carefully.

In addition, low-viscosity inks can cause a "viscous fingering" phenomenon, as discussed in **Paper I**, in combination with contact printing methods like flexography or rotogravure. Viscous fingering takes place due to hydrodynamic instability in the printing nip. This occurs in the ink transfer with a lubricating ink flow that causes unbalance between the elasticity of flexographic printing plate and the viscosity of the ink (Sauer et al. 2015).

2.3 PEDOT:PSS

Poly(3,4-ethylenedioxythiophene):poly(styrenesulfonate) (PEDOT:PSS) is a solution-processable and water soluble conductive polymer that offers

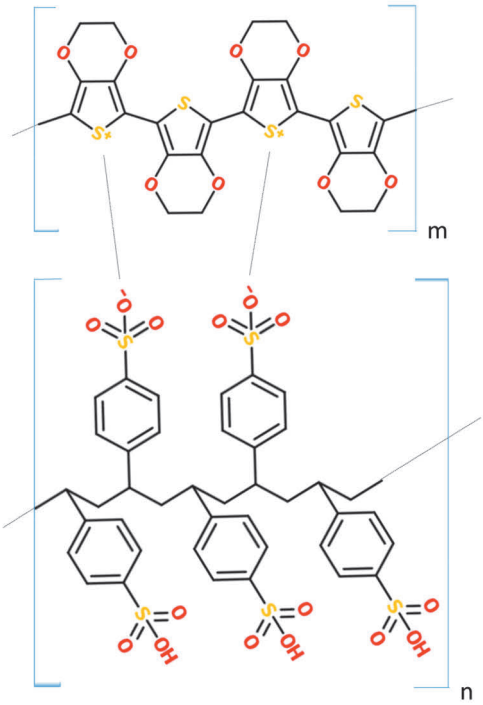

Figure 2.1 *The polymer complex comprising PEDOT (top) and PSS (bottom).*

flexibility, high transparency, high thermal stability, low production cost, and compatibility with aqueous solution-based deposition techniques. PEDOT:PSS comprises a conductive PEDOT with a PSS, as presented in Fig. 2.1. The highly conductive, hydrophobic cationic PEDOT polymer groups are adsorbed on anionic PSS polyelectrolyte chains. In the formed secondary structure, isolated PEDOT and PSS components are present, as shown in Fig. 2.2. PSS is a strong polyelectrolyte, i.e., it is fully charged in solution and dissociates well in water. Mixing the secondary structure with water induces formation of colloidal particles (tertiary structure) consisting up to 90–95% of water with hydrophobic PEDOT groups being pushed into the centre of the particle surrounded by water and anionic PSS. These colloidal particles are the building blocks of conductive PEDOT:PSS films and coatings (quaternary structure) (Mochizuki et al. 2012). The two component polymer complex structure of PEDOT:PSS can be mixed in various proportions ranging from 1:2.5 (pH 1.5-2.5) up to 1:20 (pH 7.0). This proportion controls the distance between the PEDOT:PSS clusters along the PSS chain. A larger PEDOT particle distance along the PSS-chain results in weaker conductivity. The PSS may also be produced with a shorter chain length that is suitable for inkjet printing.

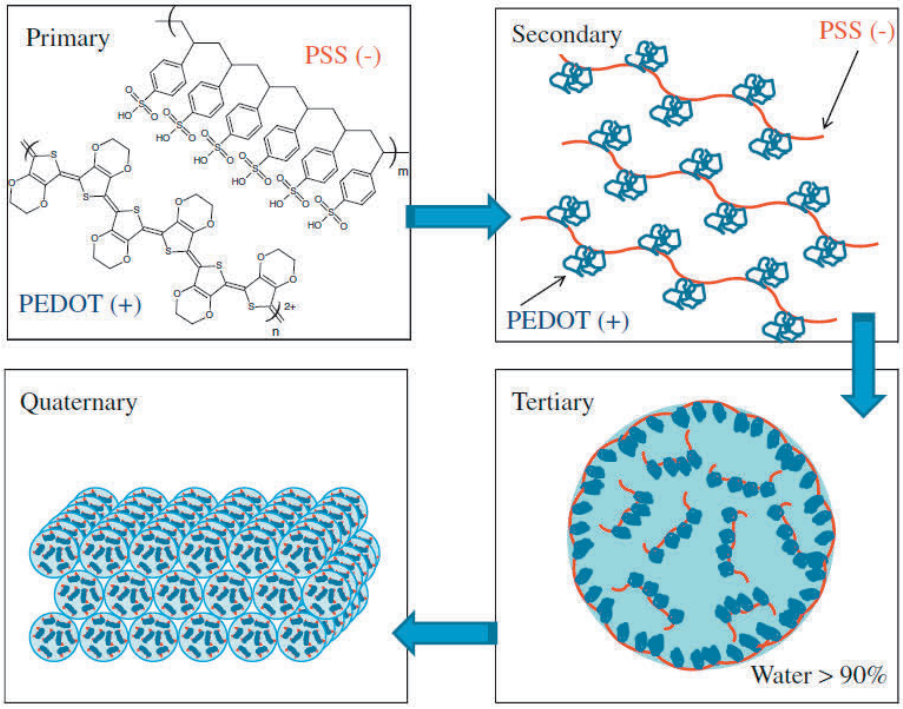

Figure 2.2 *Hierarchical structure of PEDOT:PSS (adapted from Mochizuki et al. 2012). (**Paper II**)*

The semi-transparent character of PEDOT:PSS coatings makes them suitable for optical and photonic applications. PEDOT alone found applications in capacitor production a few years earlier, but considerable difficulties with the solubility and processability prevented PEDOT from gaining a wide acceptance despite several attempts to modify the polymer structure into a more accessible form. However, PEDOT:PSS was originally developed to meet the needs of the photographic industry (Jonas & Krafft 1990). By the end of the 1980's, a few photographic film manufacturers had incorporated semi-transparent antistatic coatings into their photographic film material to prevent dust collection due to electrostatic attraction caused by the friction. The photographic film manufacturer Agfa Gevaert, at the time a subsidiary of Bayer AG (a provider of PEDOT), had been applying Na^+ $^-$PSS top coatings on its film products (Elschner et al. 2010). The idea of bringing the oppositely charged PEDOT and PSS together helped to solve the key issues, the most important of which was solubility and processability-related problems tied with PEDOT alone as well as to improve humidity tolerance and

electrical stability. Later, with the decrease of photographic film demand, PEDOT:PSS use has shifted towards photovoltaic, LED, and touchscreen applications (Perepichka & Perepichka 2009, Elschner et al. 2010).

The functionality of field effect transistors, organic photovoltaics, and LEDs is based on charge transport. In general, an insulator becomes a semiconductor when free charge carriers are generated by doping, optical excitation, or injection from electrodes. Electron mobility describes the ability of electrons to travel through metals or semiconductors. Random motion of electrons becomes directional and accelerated under the influence of an applied electric field. Analogously, hole mobility describes how holes travel in semiconductors. Charge carrier mobility (μ) combines both electron and hole mobilities in semiconductors. Hence, conductivity (σ) is a product of the elemental charge (e), charge carrier mobility (μ), and the density of charge carriers for both electrons (n) and holes (p). In semiconductors, both charge carrier species are present (Elschner et al. 2010):

$$\sigma = en\mu_e + ep\mu_h. \tag{2.1}$$

Dispersed PEDOT:PSS consists of both reduced ($PEDOT^0$) and oxidized ($PEDOT^+$) species (Andersson et al. 2002). Injected free electrons recombine at the oxidized $PEDOT^+$ site that reduces their contribution of the electron transport to the current. Thus, the charge transport is defined by the holes alone.

During a redox reaction (Eq. 2.2)

$$\underset{(red.)}{PEDOT^0} + H^+PSS^- \rightleftarrows \underset{(ox.)}{PEDOT^+PSS^-} + H^+ + e^-, \tag{2.2}$$

the PEDOT configuration will change from a chain coil structure (benzoid) of $PEDOT^0$ to a linear or extended structure (quinoid) $PEDOT^+$ (Logothetidis 2014). This will generate a charge transition from hole polarons to bipolarons. The hole polarons are positive charge carriers at the benzoid monomers, while the bipolarons are made of two positive charge carriers located along the oxidized quinoid chains (Ouyang et al. 2004). The bipolaron charge carriers are free to move along the oxidized $PEDOT^+$ and simultaneously are balanced by the counter anion in PSS^-. PSS functions as a dispersing agent to the hydrophobic PEDOT, but the PSS has also a second function: it provides (primary) dopant ions to compensate the charges of the doped PEDOT cations.

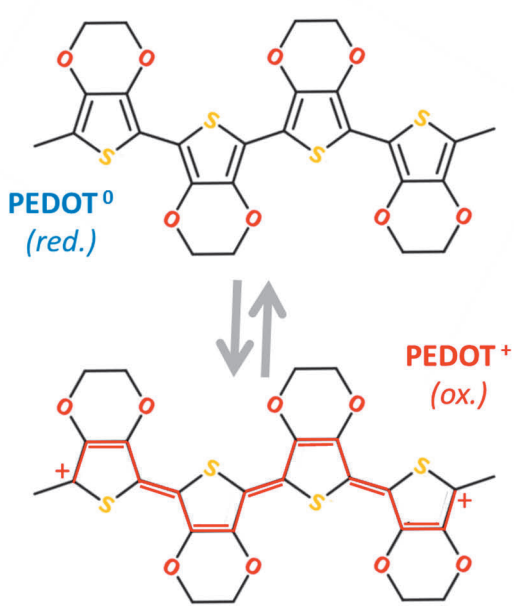

Fig. 2.3 *The PEDOT structures: benzoid (upper) and quinoid (lower).*

The more oxidized the $PEDOT^+$ becomes, the more positive hole polarons are generated for charge transport and, thus, higher conductivity is observed. Reversibly, addition of protons and electrons will reduce PEDOT and thus reduce the number of hole polarons that make PEDOT:PSS less conductive.

There is also a strong correlation between the conductivity and the opacity of the PEDOT:PSS film, i.e. transparency is reduced as the conductivity increases. Opaqueness is commonly a problem, but relatively high transparency has been demonstrated with high conductivity (Kim et al. 2011, Vosgueritchian et al. 2012) for replacing brittle and expensive indium tin oxide (ITO) films for photovoltaic applications. Recently, a solar cell (Hu et al. 2013) and an OLED device (Zhu et al. 2013) were created using a spin-coated conductive PEDOT:PSS on NFC substrate. Additionally, PEDOT:PSS has been used with carbon nanotubes (CNTs) in a layer-by-layer coating of wood microfibers for paper-based batteries (Aliahmad et al. 2013) and capacitors (Agarwal et al. 2009).

The conductivity of PEDOT:PSS can be improved by an acid treatment (Howden et al. 2013, McCarthy et al. 2014) or by additives such as poly-alcohols, e.g. glycerol (Ouyang et al. 2005), solvent (Yan et al. 2011), or polyelectrolytes (Valtakari et al. 2015). In papermaking, polyelectrolytes are

traditionally employed as retention aids in the wet-end of the manufacturing process, and as dispersing agents in paper coatings (Alén 2007). The mineral pigment paper coatings are typically covered by a monolayer of polyelectrolytes (Koivula et al. 2011). It is essential from the paper electronics design point of view to understand the potential interactions between the paper chemicals and the functional materials used.

2.4 Nanocellulose

Nanostructured cellulose-based materials have attracted large interest within the past two decades due to their unique properties. There are several different forms, ranging from micro- or nanofibrillated cellulose (MFC/NFC) and nanocrystalline cellulose (NCC or CNC) to bacterial nanocellulose categorized according to their structure, fibre size, or production method: for an excellent review, see Dufresne (2013).

Nanofibrillar cellulose (NFC) can be utilized in various end-use products ranging from thin films, coatings, and composites to aerogels and hydrogels. NFC has fibrils with a high aspect ratio of several hundred: the fibrils are typically 5 to 20 nm in diameter while being several micrometres in length. This and the large specific surface area lead to the high strength of NFC films and coatings (Kumar et al. 2014). Recently, NFC-based conductive films and composites for electronics applications have been studied (Salas et al. 2014). NFC films have good thermal (Zhu et al. 2013, Xue et al. 2015) and barrier properties (Fukuzumi et al. 2009) with high chemical stability (Zheng et al. 2013), tuneable optical properties (Hu et al. 2013), high toughness (Salajkova et al. 2013), and low surface roughness (Torvinen et al. 2012). Therefore, NFC films can potentially be used as a substrate for flexible and transparent electronic devices for cost-effective manufacturing in a roll-to-roll process flow. Being semi-transparent, light, and strong with low oxygen permeability, NFC has significant potential as a biodegradable substitute for plastic and glass.

2.5 Liquid flame spray (LFS) nanoparticle deposition

Liquid flame spray (LFS) is a cost-effective way to deposit various metal and metal oxide nanoparticles on a large area via roll-to-roll process flow at atmospheric conditions. In LFS nanoparticle deposition, as shown in Fig. 2.4, an organometallic liquid precursor, typically dissolved in isopropyl alcohol (IPA), is fed into a high-velocity and high-temperature H_2-O_2 flame in which

the precursor evaporates, reacts, nucleates, and forms solid nanoparticles. The formed nanoparticles can be collected on various substrates from glass and steel to paper and plastic films (Mäkelä et al. 2006). The flame deposition can be combined into a R2R process flow with web speeds exceeding 150 m/min that allows several square meters of nanoparticle coated surfaces to be manufactured in a minute with a single burner nozzle. This is beneficial for highly efficient paper production, where line speeds typically vary from 300 to 2000 m/min. In contrast, throughput of photovoltaic devices demonstrated in papers (Barr et al. 2011, Hübler et al. 2011) is very limited due to very slow coating in the production process. The oxidative chemical vapour deposition (oCVD) utilized by Karen Gleeson's group (Barr et al. 2011) provided a perfect contour coating of PV cells with no electric shorts on rough paper including a tissue paper, but at the expense of a slow batch process. An all-printed PV process by Hübler et al. (2011) had a 12-hour delay between different prints and thus did not allow a continuous process flow.

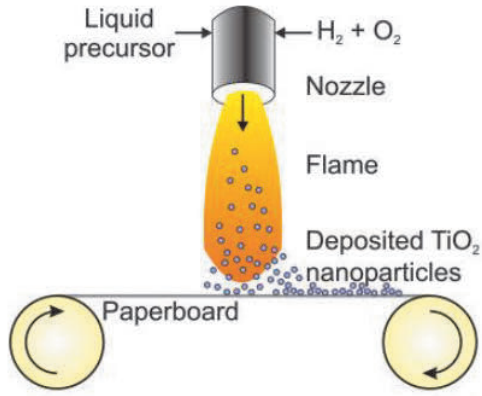

Figure 2.4 *A schematic of the LFS process used for TiO_2 nanoparticle deposition on paperboard. (**Paper IV**)*

The LFS process results in a relatively narrow size distribution of nanoparticles with a controllable nanoparticle diameter from 2 to 200 nm. The sizes of the nanoparticles can be controlled simply by changing the deposition parameters, i.e. the relative gas flow, the precursor feed rate and concentration, and the distance of the nozzle from the deposited surface (Mäkelä et al. 2004). LFS has found applications in glass colouring (Gross et al. 1999), catalytic applications (Keskinen et al. 2006), and antibacterial surfaces (Gunawan et al. 2009).

The LFS coating technique is expected to provide a cost-effective large-area roll-to-roll production of nanoparticle coated surfaces that can find applications, for example, in POC diagnostics, surface-enhanced Raman sensing (Saarinen et al. 2014, Saarinen et al. 2017) or solar cell applications.

2.6 Surface wetting

2.6.1 Wetting of surfaces

The liquid drop is wetting the surface if it spreads across the surface and makes a good contact with the solid surface. The axisymmetric drop shape formed on the solid surface is defined by two key parameters: the surface tension of the liquid and its contact angle (CA). CA is the angle formed at the solid-liquid-vapour along the three-phase contact line once the liquid drop has reached its equilibrium with the surrounding vapour phase, as depicted in Fig. 2.5.

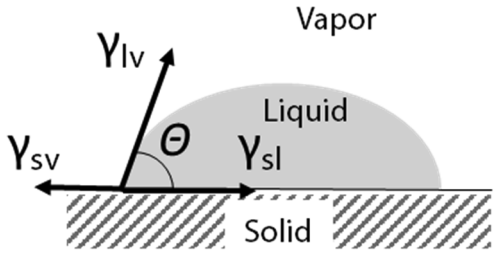

Figure 2.5 *A sessile drop on a solid surface.*

The equilibrium of a drop deposited onto a surface is described by the classical Young's equation (Young 1805, Ullman 1995, van Oss 2006)

$$\gamma_{\mathrm{lv}} \cos\theta = \gamma_{\mathrm{sv}} - \gamma_{\mathrm{sl}}, \tag{2.3}$$

where γ_{lv}, γ_{sv}, γ_{sl}, and θ are the liquid-vapour, solid-vapour, and solid-liquid interfacial tensions and the CA. Of the four parameters, γ_{lv} and θ can be measured easily, which increases the usability of Young's equation. The surface wetting and the drop contact with the solid surface are increased with lowered contact angle, and vice versa. Solid surfaces with water contact angle (WCA) values smaller than 90° are categorized as hydrophilic surfaces, and for values greater than 90° as hydrophobic surfaces. Addition of wetting agents or

surfactants to water will lower the surface tension. Thus, the WCA in contact with a hydrophilic surface will decrease, resulting in improved wetting. The other two parameters in Young's equation, γ_{sv} and γ_{sl}, are used to describe the behaviour and properties of paints, adhesives, detergents, and lubricants.

Young's equation assumes that the sessile drop stays in contact with an ideally smooth, homogeneous, isotropic, and non-deformable surface. Unfortunately, the real-world surfaces clearly deviate from these assumptions. For rough surfaces, this issue was addressed by the introduction of a roughness ratio factor r by Wenzel already in 1936 (Wenzel 1936). A rough surface area covers more space due to surface variations providing a higher surface area compared to an ideally smooth surface that is represented by a geometric surface area. The roughness value r is the ratio of these two areas as follows:

$$r = \frac{\text{actual surface area}}{\text{geometric surface area}} \ . \tag{2.4}$$

The interfacial tensions γ_{sv}, and γ_{sl} that refer to the geometric area in Young's equation are redirected to the actual surface area in the Wenzel equation

$$\gamma_{lv}\cos\theta_W = r(\gamma_{sv} - \gamma_{sl}), \tag{2.5}$$

where θ_W designates the Wenzel CA. For heterogeneous surfaces, the Cassie CA θ_C applies (Cassie & Baxter 1944). Therefore, the Cassie equation for a two-component composite with two different interfacial tension domains is given by

$$\cos\theta_C = a_1\cos\theta_1 + a_2\cos\theta_2, \tag{2.6}$$

$$a_1 + a_2 = 1, \tag{2.7}$$

where θ_1 and θ_2 are the intrinsic CAs on the fractional surface areas, a_1 respectively a_2. Originally, the Cassie equation was developed for porous systems with one component representing a solid and the second one being air, i.e. $\theta_2 = 180°$ and $\cos\theta_2 = -1$. For a small solid fractional surface area, a_1, with effective CA, θ_1, the Cassie equation then becomes

$$\begin{aligned}\cos\theta_C &= a_1\cos\theta_1 + (1 - a_1)(-1)\\ &= a_1\cos\theta_1 + (a_1 - 1)\\ &= a_1(\cos\theta_1 + 1) - 1.\end{aligned} \tag{2.8}$$

This results in a very large θ_C that is caused by the water-repelling quality of the air/solid composite structure. The main principle of superhydrophobic surfaces, such as the LFS TiO_2 nanoparticle coated paperboard used in this work in **Papers I** and **IV**, is based around the principles of Eq. 2.8. Wenzel (Eq. 2.5) and Cassie (Eq. 2.6) equations apply to a sufficiently large drop size in proportion to the roughness scale of the surface.

2.6.2 Controlled wetting

The ability to control wetting is essential in various applications, from printing and coating to painting and laminating. This can be achieved through several nanoscale surface modification methods, such as plasma treatment and vapour deposition methods. In plasma surface treatment, activated plasma species initiate chemical and physical reactions at the substrate surface (Biederman 2004). Plasma is a result of applied energy into gas that dissociates gas atoms and molecules into charged species including electrons, ions, molecules, and radicals (Tendero et al. 2006). The used plasma process parameters depend on the gas type, energy source, and ionization mechanism (Friedman 2008, Cernakova et al. 2006). With oxygen gas, the charged oxygen plasma species at the substrate surface significantly increase the polar component of the surface energy converting the substrate surface into a more hydrophilic state. The corona discharge method forms a special subcategory of plasma surface treatments at ambient conditions in which a high voltage plasma is generated in the proximity of a pair of large surface area metal electrodes. When the planar substrate is fed in between the electrodes in an electrical discharge gap, the oxygen of air dissociates into charged oxygen species. Corona discharge is a popular surface modification method widely employed in the paper converting industry for improved coatability (Bollström et al. 2012), printability (Pykönen et al. 2008), and adhesion between polymer and paper substrates (Vähä-Nissi et al. 1997).

Evaporation-based surface modification methods typically exhibit initiated film growth by nucleation followed by grain growth that eventually coalesce into a continuous film with a 5-10 nm thickness (Green 1994, Dana et al. 1992). Chemical vapour deposition (CVD), physical vapour deposition (PVD), atomic layer deposition (ALD), and liquid flame spray (LFS) deposition methods fall into this category.

ALD can be divided into sequenced self-saturating deposition cycles. This results in a continuous layer-by-layer film growth with a single layer at a time

(Ritala & Leskelä 2001), and such an approach can provide unique film properties. CVD and PVD films typically exhibit compressive stress with pinholes associated with non-ideal grain boundaries that make these films unsuitable for passivation and encapsulation applications with film thickness less than 500 nm. ALD, however, can produce films without nucleation-related discontinuities that result in a pinhole-free and stress-free film structure suitable for very thin encapsulation films (Sneh et al. 2002).

In LFS nanoparticle deposition, controlled wettability of a paperboard can be achieved using TiO_2 nanoparticles (Mäkelä et al. 2011) that can be controlled via ultraviolet A (UVA) radiation and a heat treatment (Teisala et al. 2013, Stepien et al. 2011). TiO_2 is a semiconductor that allows controlled wettability via photocatalytic activation. The band gap energy of TiO_2 anatase crystalline form is 3.2 eV (Schneider et al. 2014) that corresponds to 387 nm, i.e. photons with shorter wavelength than this value can lift electrons from the valence band into the conduction band. In nanostructured media, both holes in the valence band and the added electrons in the conduction band can easily diffuse onto the surface leading to its high reactivity.

Well-known photocatalytic properties of TiO_2 (Fujishima et al. 2000, Caputo et al. 2008) can be used to convert the TiO_2 nanoparticle coated paperboard surface from superhydrophobic to a highly hydrophilic one under ultraviolet (UVA) light. A similar photocatalytically induced wettability conversion from superhydrophobicity (WCA > 150°) to high hydrophilicity (WCA < 20°) has been observed on TiO_2 nanoparticle coated paperboard surfaces (Stepien et al. 2011, Stepien et al. 2013). Exposure to a UV source triggers a photocatalytic wettability conversion from hydrophobic to hydrophilic, whereas a thermal treatment has a reverse effect restoring the wettability back to the initial superhydrophobic state.

Using a photomask with UVA light, various patterns with differing and controlled wettability can be formed on TiO_2 nanoparticle coated paperboard surface. The observed changes in the wettability correlate well with the changes in the surface chemistry, as verified by X-ray photoelectron spectroscopy (XPS) (Stepien et al. 2012) and time-of-flight secondary ion mass spectrometry (ToF-SIMS) (Stepien et al. 2013) studies. Nevertheless, the induced wettability conversion is reversible: the surface recovers the initial hydrophobicity level at ambient conditions in dark during storage. The recovery of the hydrophobicity can be enhanced by external heat. This recovery of the wettability is a problem especially for fabrication of microfluidic POC devices, since it limits the product's shelf life.

Chapter 3

Materials and Methods

3.1 Substrates

3.1.1 Multilayer coated paper (MLCP)

PEDOT:PSS was printed using flexography on multilayer pigment coated specialty paper developed at Åbo Akademi University for printed functionality applications (Bollström et al. 2009). The multilayer coated paper (MLCP) consists of a double-coated base paper (commercial fine paper Lumipress 115, StoraEnso, FI) on which a 10 g/m^2 barrier layer mixture of platy kaolin (Barrisurf HX, Imerys Minerals Ltd, UK) blended with 50 pph ethylene acrylic latex (Aquaseal 2077, Paramelt B.V., NL) is coated to prevent ink penetration. Printability of functional inks is adjusted by a 5 g/m^2 topcoating layer consisting of a blend of 70 pph fine platy kaolin (Barrisurf FX, Imerys Minerals Ltd. UK) and 30 pph fine blocky kaolin (Alphatex, Imerys Minerals Ltd., UK) with 6 pph SB latex binder (Basonal 2020.5, Basf, DE). The paper is calendered three times in a softnip calender with a line load of 120 kN/m and a temperature of 70 °C to achieve final smoothness comparable to a Mylar A plastic film. More details about the manufacturing of the MLCP substrate can be found in Bollström et al. (2009).

3.1.2 Paperboard coated with TiO_2 nanoparticles

TiO_2 nanoparticles were deposited on paperboard with a liquid flame spray (LFS) coating method in a R2R process (Mäkelä et al. 2011). In this process, the paperboard passes at a high speed under a high temperature flame in which an organometallic liquid precursor evaporates, reacts, nucleates, and forms solid nanoparticles. The formed nanoparticles are collected on the moving paperboard surface. A double pigment coated paperboard (200 g/m^2, Stora Enso, Skoghall, SE) was coated using the converting pilot line at Tampere University of Technology (Tampere, Finland) with a web speed of 30 m/min. Liquid titanium(III)isopropoxide (TTIP) dissolved in isopropanol with a metal ion concentration of 11.9 mg/ml was fed with a 29.5 ml/min feeding rate into the nozzle whose distance from the moving web was set to 15 cm. This resulted in a 12.7 mg/m^2 deposition mass of nanoparticles, and the average nanoparticle

diameters ranged from 40 to 80 nm with surface coverage of ca. 415 TiO_2 nanoparticles per μm^2 (Stepien et al. 2011). Such substrate was used in **Paper I** to study the printing of PEDOT:PSS conductive layers on TiO_2 coated paperboard as such and also via photocatalytically activated wettability conversion. Additionally, a two-stage successive wetting characteristic of the TiO_2 nanoparticle coated paperboard was studied in **Paper IV** that resulted in a formation of permanent planar fluidic channels.

3.1.3 Nanofibrillated cellulose (NFC)

The NFC suspension was prepared from bleached birch Kraft pulp using 2,2,6,6-tetramethylpiperidine-1-oxyl (TEMPO)-mediated oxidation followed by mechanical disintegration, as reported by Liu et al. (2014). Ten grams of the pulp fibres were dispersed in 600 mL deionized (DI) water (Millipore 18.2 Ω). The TEMPO (0.1 mmol/g fibre) and NaBr (1.0 mmol/g fibre) were dissolved in 300 mL DI water and then mixed with the pulp slurry. The concentration and the pH of the pulp were adjusted to 0.1% and 10.0, respectively. The oxidation was started by adding the NaClO (10 mmol/g fibre) solution dropwise. All NaClO solution was added in 8 h. During the reaction, the pH of the reaction mixture was kept at 10.5 by adding 0.5 M NaOH. After 24.0h reaction, the mixture was precipitated in ethanol and purified three times by washing with DI water and centrifugation at 3500 rpm for 10 min. The oxidized fibres were diluted to a concentration of 0.5% and mechanically fibrillated with a domestic blender (OBH Nordica 6658, Denmark) for 5 min. The carboxylate content (1.79 ± 0.11 mmol/g) of the resulting NFC was determined by conductometric titration (Liu et al. 2014). All chemicals (Sigma Aldrich, St. Louis, USA) were used without further purification.

The NFC and glycerol (≥99.0%, Sigma-Aldrich, St. Louis, USA) solutions (NFC-G) were prepared by weighing and diluting to given strengths using DI water and small 1.5 mL microcentrifuge tubes. All NFC-G coatings were well mixed and applied fresh on the surface immediately after the mixture preparation.

3.1.4 Plastic film

A commercial poly(ethylene terephthalate) (PET) film is a low-cost, semi-transparent, and flexible, roll-to-roll compatible film. PET (Mylar ®A, Dupont Teijin Films) was used as a reference plastic film in **Paper I** in which

flexographic PEDOT :PSS prints on multilayer coated paper, paperboard, and TiO_2 nanoparticle coated paperboard were compared.

3.1.5 Glass

Cut and cleaned microscope glass slides (Menzel Gläser/Thermo Scientific by Gerhard Menzel GmbH, DE) made of extra-white soda-lime glass with very low iron content (0.03% Fe_2O_3) were used in **Papers II** and **III**. Glass substrate eliminates additional variables and complexity induced by rough and porous coated paper substrates, i.e. the wide variability of coating pigment particle mixtures with varying absorption, porosity, and surface roughness characteristics.

3.2 Inks and coatings

3.2.1 PEDOT:PSS

Two different types of commercially available PEDOT:PSS were used in this work: in **Paper I**, a standard, homogenized Clevios PH500 (Heraeus GmbH, Leverkusen, DE) for printing, and in **Papers II** and **III**, a more viscous Clevios P HC V4 (Heraeus GmbH, Leverkusen, DE) for spin-coating.

3.2.2 Polyelectrolytes

The interaction between the conductive polymer PEDOT:PSS and anionic sodium polyacrylate (PA, molecular weight < 10 kDa, Polysalz S, BASF, DE) or cationic (poly-DADMAC, molecular weight > 80 kDA) was studied in **Paper II**. Both polyelectrolytes were coated on clean glass slides by spin-coating.

3.2.3 Silver

Silver conductive paint (Electrolube, Derbyshire, UK) was used in conductivity measurements of the PEDOT:PSS in **Papers I**, **II**, and **III**. The sheet resistance was measured over two parallel hand-painted highly conductive silver paint contacts with inner borders 10 mm apart from each other.

3.3 Sample Preparation Techniques and Procedures

3.3.1 Flexography

Figure 3.1 *A laboratory scale flexography IGT GST 2 printability tester.*

Flexography is a traditional contact printing method that has achieved a widespread popularity especially in the packaging industry. In flexography, the ink is spread over an anilox cylinder, i.e. a metal or a ceramic cylinder having engraved, uniformly distributed cells. The anilox cylinder dispenses the ink evenly onto an impression roller that will transfer the designed pattern onto the substrate surface. In graphic printing, the print pattern is a raster image made of discrete dots. A wide range of anilox cylinders exist with mechanically or laser engraved cells in different sizes and/or shapes (Kipphan 2001). Cells with larger volumes provide a larger transfer volume capability and a lower resolution. Flexography inks are thicker and more viscous than inkjet inks but thinner than tackier off-set and silkscreen inks. The viscosity of flexographic inks is typically in the range of 300 ± 200 mPas. Excess pressure between the impression cylinder and the printed surface results in compression of the ink and loss of definition in the print pattern edges, known as a halo-effect. The pressure between the anilox cylinder and the printing plate as well as the pressure between the printing plate and the substrate was set to 50 N. In **Paper I**, flexographic printing of PEDOT:PSS was performed on various substrates using a IGT Global Standard Tester 2 (IGT Testing Systems, Amsterdam, NL)

with an anilox cylinder with a volume of 20 ml/m^2 and 40 lines/cm, as shown in Fig. 3.1.

3.3.2 Spin coating

Spin-coating is a conventional method for applying thin films on small flat and rigid substrates. The process can be described in three main steps: i) deposition of a small amount of solution onto the substrate face, ii) a spinning step (speeds ranging from 1 000 to 8 000 rpm), and iii) the drying step. In the spinning step, centripetal forces will leave a thin film on the substrate surface forcing the excessive liquid off the edge. The resulting film thickness is mainly determined by the viscosity of the solution, the spinning rate, and the drying rate. Along the static dispense method described above, a dynamic dispense method can also be applied to solutions or substrates having a poor wettability. In the dynamic dispense method, the initial spinning rate is kept at low levels (approximately at 500 rpm) for a few seconds to retain as much solution at the substrate surface as possible. This is followed by a high-speed spinning step that will thin out the film to its final thickness. Spin-coating is suitable for fast and simple prototyping. Furthermore, spin-coating has excellent repeatability for parallel sample preparation and reproducibility within very narrow margins. This is especially important for multilayer construction, where every additional processing step and layer is a potential source of error.

Figure 3.2 *The KW-4A spin coating unit.*

In this work, the spin-coating was performed using a spin-coater unit (KW 4A, Chemat Technology Inc., USA) shown in Fig. 3.2. In **Paper II**, the polyelectrolytes were spin-coated onto hand cut 2.5 × 2.5 cm^2 glass slides for

60 s at 1050 rpm for PA and 1300 rpm for pDADMAC with the following concentrations: PA at 2.5 wt.%, 5 wt.%, and 10 wt.%, and pDADMAC at 1 wt.%, 2.5 wt.%, 5 wt.%, and 10 wt.%. For the NFC film deposition in **Paper III**, the glass slide surfaces were first oxygen plasma treated (O_2^+, O_2^-, O_3, O, O^+, and O^- species) in the etch mode in a high vacuum sample sputter coater (SCD 050, Bal-Tec AG, Balzers, LI; now Leica Microsystems GmbH., Wetzlar, DE) for 60 s at 20 mA and 0.05 mbar vacuum pressure for 3–15 min prior to spin coating. The plasma treatment lowered the WCA (KSV Cam 2000, Biolin Scientific Inc., Espoo, FI) on the glass surface from 14° to 0°. In **Paper III**, the glass substrate was oxygen plasma activated before glycerol application to promote adhesion. For applying a conductive PEDOT:PSS layer in **Papers II** and **III**, homogenized standard PEDOT:PSS was spin-coated on top of the polyelectrolyte film or NFC films before annealing following the parameters given in **Papers II** and **III**.

3.3.3 Drop cast NFC films

In drop casting a substrate surface is covered with a solution and left to dry. The drying rate and the film thickness are controlled by the composition of the solution, dry content, and viscosity. The drop casting technique was used to produce NFC and NFC-G coatings in **Paper III**.

3.3.4 PEDOT:PSS on polyelectrolyte coated substrate

The effect of cationic pDADMAC and anionic PA polyelectrolytes on PEDOT:PSS conductivity was studied in **Paper II**. The polyelectrolyte solutions were spin-coated on 2.5 × 2.5 cm^2 glass slides for 60 s at 1050 rpm for PA and 1300 rpm for pDADMAC with the following concentrations: PA at 2.5 wt.%, 5 wt.%, and 10 wt.%, and pDADMAC at 1 wt.%, 2.5 wt.%, 5 wt.%, and 10 wt.%. PEDOT:PSS was deposited by spin-coating on top of the polyelectrolyte layers. The PEDOT:PSS spin-coated samples were annealed at 130°C for 15 min and stored overnight at RH 50%. The sheet resistance was measured across two hand-painted silver electrodes 10 mm apart. The print density values were measured using an optical densitometer (Techkon, SpectroDens, DE) from three different locations within the 1.0 × 1.0 cm^2 area used for the sheet resistance measurements.

3.3.5 PEDOT:PSS on NFC-G coated substrate

The effect of NFC on PEDOT:PSS conductivity was studied in **Paper III**. Two different approaches were taken to deposit PEDOT:PSS on NFC-G coatings either by spin-coating or drop cast coating, as presented in Fig. 3.3. Although it is hydrophilic, NFC does not adhere onto glass substrate to form flat, uniform films. Therefore, the cleaned glass substrates 2.5 × 2.5 cm^2 were oxygen plasma treated to create temporary high hydrophilicity allowing the NFC-G mixture to adhere on the glass surface. A spin-coated glycerol (anchor) layer improved the overall uniformity of the NFC-G coating. The drop cast samples were produced by spreading an additional (drop-cast) NFC-G layer on a pre-coated NFC-G layer and were left to dry for 24h. Finally, all the samples were spin-coated with a PEDOT:PSS layer, annealed at 60-130°C for 20 min, and stored overnight at RH 50% before measurements. The sheet resistance was measured across two hand-painted silver electrodes 10 mm apart.

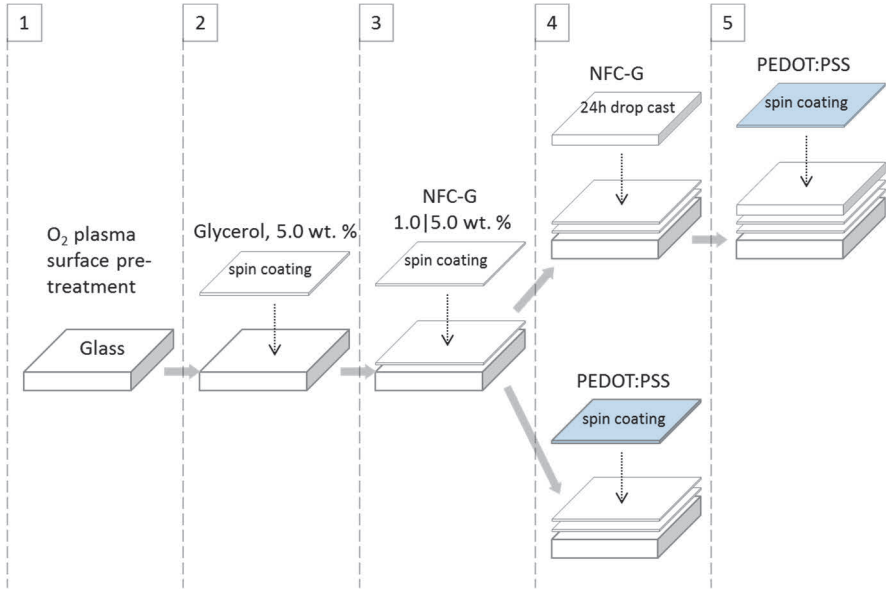

Figure 3.3 *Two different sample preparation approaches for PEDOT:PSS on NFC-G film.*

3.3.6 TiO_2 nanoparticle coated paperboard wettability conversion

Photocatalytic wettability conversion was utilized in **Papers I** and **IV**. The TiO_2 nanoparticle coated paperboard surface was exposed to UV irradiation using a UV light source (Bluepoint 4 Ecocure, Hönle UV Technology, Gräfelfing, DE) with a UVA filter having a 365 nm central wavelength under a passband filter for 320-390 nm. The exposure intensity was constant (50 mW/cm^2) with 30 min exposure time. It has been shown earlier (Stepien et al. 2011) that the selected UVA exposure time converts the initially superhydrophobic TiO_2 nanoparticle coated surface into a highly hydrophilic one. The observed UVA induced hydrophilicity conversion is not permanent, and the superhydrophobicity recovery can be enhanced by a heat treatment in an oven at 150°C for 3 min (Stepien et al. 2012).

3.3.7 Permanent planar fluidic channel preparation on TiO_2 nanoparticle coated paperboard

Permanent planar fluidic channels on TiO_2 nanoparticle coated paperboard were developed in **Paper IV**. To make the UVA illuminated channel structure permanent, the channel area was exposed to water in the first stage wetting, as shown in Fig 3.4. The first stage wetting removes TiO_2 nanoparticles from the hydrophilic channel area. Two samples were prepared: with and without the first stage wetting. Both samples were then heat treated in an oven at 150°C for 3 min. Without the first stage wetting the TiO_2 nanoparticles remain on the paperboard surface at the illuminated channel area and, thus, convert back to superhydrophobic by the heat treatment. The second stage wetting only occurs in the first stage wetted channel, as shown in Fig. 3.4. Both samples were kept at 24°C and at RH 50% overnight after the heat treatment before the wettability measurements.

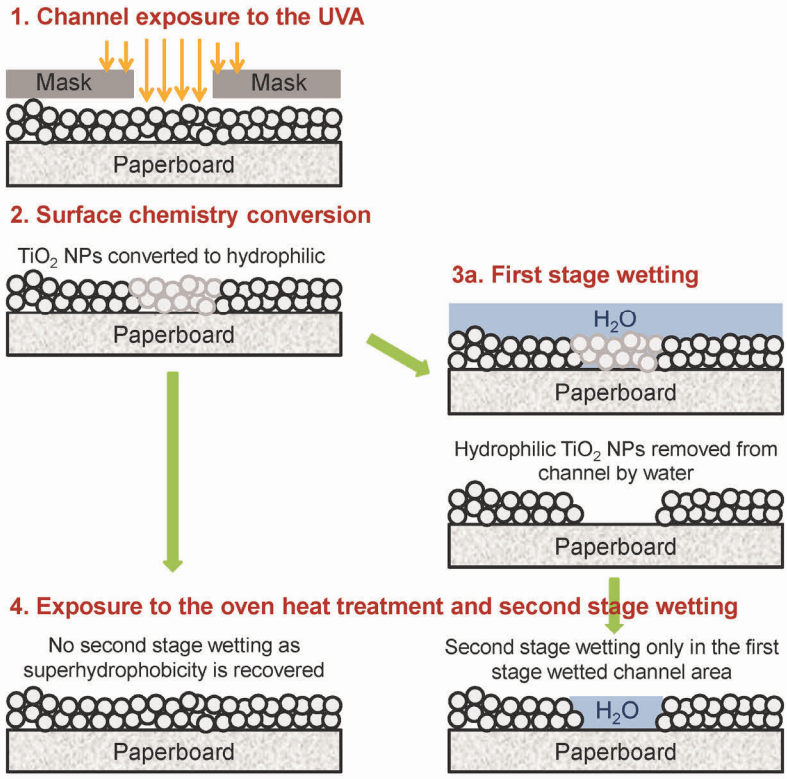

Figure 3.4 *A schematic of the permanent planar channel preparation using a two-stage wetting process with the UVA illuminated channel structures.*

3.4 Sample Characterization Techniques

3.4.1 Sheet resistance

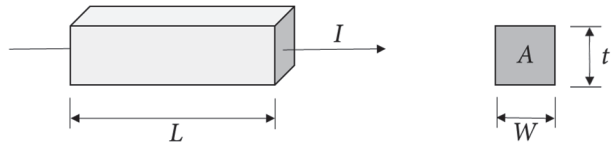

Figure 3.5 *Sheet resistance measurement.*

Sheet resistance R_S is the ratio of the resistivity to thickness of the material (Jaeger 2002) given by

$$R = \rho \frac{L}{A} = \left(\frac{\rho}{t}\right)\left(\frac{L}{W}\right) = R_s\left(\frac{L}{W}\right), \tag{3.1}$$

where ρ, L, and A represent the resistivity, length, and cross-sectional area of the material, respectively. The number of unit squares (□) in the material is represented by the ratio L/W that has no unit. Therefore, sheet resistance is a practical tool for resistance measurements allowing for a comparison of materials with different physical size, as shown in Fig. 3.5. In this work a digital multimeter (Keithley 2100, US) was used for sheet resistance measurements of flexography printed PEDOT:PSS in **Paper I**, spin-coated PEDOT:PSS on polyelectrolyte layers in **Paper II**, and spin-coated PEDOT:PSS on spin-coated or drop cast NFC-G layers in **Paper III**.

3.4.2 Water contact angle (WCA): Sessile drop technique

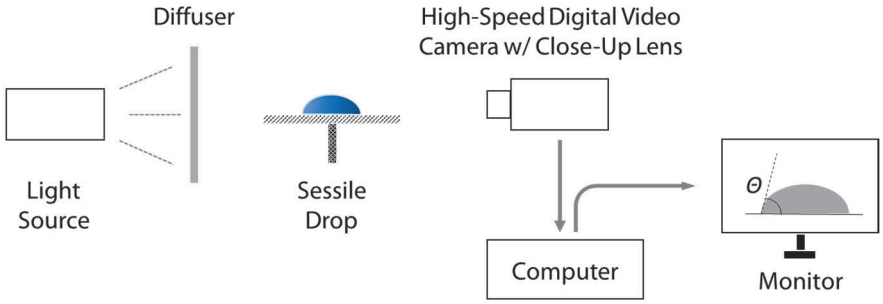

Figure 3.6 *A sessile drop CA measurement setup.*

The sessile drop technique is a classical wetting study technique. An optically enlarged profile of a liquid drop deposited onto a solid surface is measured against a uniformly illuminated background, as shown in Fig. 3.6. A contact angle goniometer (KSV CAM 2000, Biolin Scientific Ltd., Espoo, FI) was used in **Papers I**, **III**, and **IV**.

3.4.3 Optical transmission and print density

An ordinary transmission spectrometer is based on the Beer-Lambert law that relates the passing or reflecting light intensity I to the intensity of the beam I_0

$$I = I_0 \exp(-\alpha d), \tag{3.2}$$

where the absorption coefficient α is multiplied by the geometrical length d. Transmission T of a material is the ratio of these beams and is related to the print density D as follows:

$$T = \frac{I}{I_0} = \exp(-\alpha d) = 10^{-D}, \tag{3.3}$$

$$D = -\log_{10}(T) = -\log_{10}(\exp(-\alpha d)). \tag{3.4}$$

PEDOT:PSS printed and coated samples were studied using an optical densitometer in **Papers I**, **II**, and **III**. Optical densitometers are designed to measure the light intensity and colour readings with a spectral scanning head indirectly, i.e. using reflected light from the sample surfaces. A density value of 0.0 refers to a perfect reflector, whereas a density value of 3.0 refers to only 0.01 (1%) reflection. Thus, a printed area with a reflection of 0.1 (10%) yields a print density of 1.0. There are several practical reasons for using print density values instead of ordinary transmission spectroscopy: inks and, in this work, semi-transparent PEDOT:PSS layers correlate well with the relative layer thicknesses. An optical densitometer (SpectroDens, Techkon GmbH., DE) was used to measure ink density for non-transparent samples in **Paper I** and for semi-transparent substrates in **Papers II** and **III**.

3.4.4 Scanning electron microscopy (SEM)

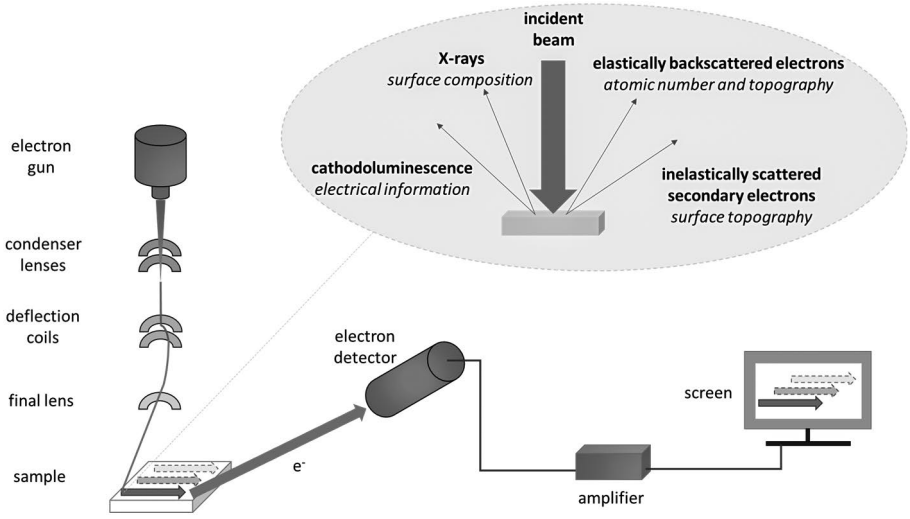

Figure 3.7 *A SEM measurement setup.*

The SEM (Fig. 3.7) is a high resolution imaging instrument for vacuum compatible materials that can provide accurate information about the structure and composition of a material. Samples are studied under an ultra-

high vacuum condition. They are also subject to damage caused by the high intensity electron beam while scanning back and forth and interacting with the sample surface. The common signals include inelastically scattered secondary electrons, elastically back-scattered electrons, and X-ray photon emission that originate from the inelastic and elastic interaction of the electron beam with the sample. The detected signals are modulated and A/D-converted to modern display standards providing magnified microscopic images with a large depth of field from the area localized directly under the electron beam. Lateral resolution in the range of 1-50 nm can be achieved in secondary electron mode. Besides structural analysis, the SEM instrument can also be suitable for elemental analysis. However, no chemical bonding information is available. Non-conductive samples must be coated with a conductive film prior to imaging. In this work, samples were imaged for coating thickness and composition analysis. A field-emission SEM with in-lens detector (LEO Gemini 1530, Zeiss Microscopy GmbH., Oberkochen, Germany) located at the Laboratory of Inorganic Chemistry, Åbo Akademi University was used in **Papers II**, **III**, and **IV**.

3.4.5 X-ray photoelectron spectroscopy (XPS)

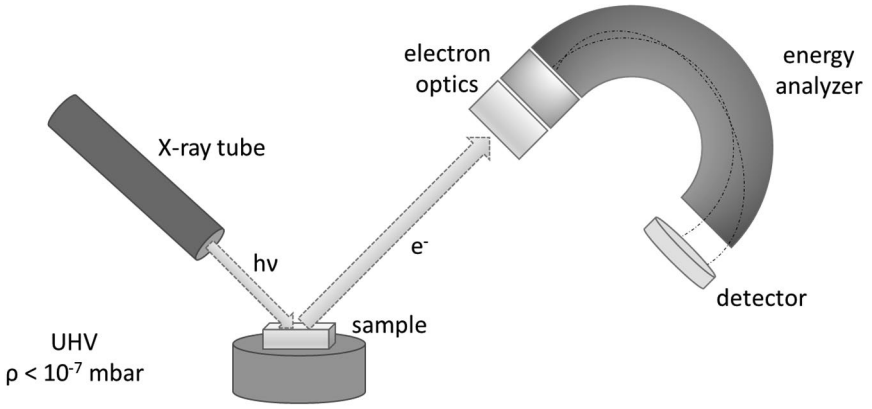

Figure 3.8 *An XPS measurement setup.*

XPS (Fig. 3.8) was utilized in **Paper IV** to study the surface chemical changes induced by the first stage wetting of LFS TiO_2 nanoparticle coated paperboard. XPS is a tool for highly surface sensitive studies of inorganic and organic surface compositions and electronic structures. The sample is bombarded with

a focused monoenergetic soft X-ray beam that releases photoelectrons from the surface. For a qualitative chemical analysis, all elements excluding hydrogen and helium present at the surface can be detected by the emitted photoelectrons and their respective kinetic energies that reach the detector. For a quantitative analysis, the relative concentrations of the elements are calculated from the detected photoelectron intensities. The probing depth is 2-20 atomic layers or 5-50 Å, depending on the material and the take-off angle, with a 5 to 75 μm lateral resolution (Ullman 1995). The sample has to be compatible with ultra-high vacuum conditions. X-ray sensitive materials may also suffer damage induced by the beam.

To study the surface chemistry of the TiO_2 channel structures in **Paper IV**, XPS measurements were performed using a PHI Quantum 2000 instrument (Physical Electronics Instruments, USA) with a monochromatic Al Kα X-ray source operated at 25 W. Charge compensation was improved by a combination of electron flood and ion bombarding. A take-off angle of 45° relative to sample surface was used. High-resolution photoemission peaks for C 1s, O 1s, and Ti 2p were measured from three different spots using a pass energy of 29.35 eV. A mixed Gaussian–Lorentzian fit and Shirley background reduction were used for curve fitting. The main chamber pressure was kept at 2×10^{-7} Torr during the measurement.

3.4.6 Time-of-flight secondary ion mass spectrometry (ToF-SIMS)

ToF-SIMS mapping (Fig. 3.9) of the paper sample was used in **Paper IV** to study the changes caused by both UVA irradiation and/or water wetted LFS TiO_2 nanoparticle coated paperboard. ToF-SIMS provides elemental and molecular level information at high spatial resolution with an imaging depth of 1-2 nm. It is therefore well suited for characterization of the molecular distribution at the outermost surface (Dalton et al. 2002, Stepien et al. 2013). The sample surface is bombarded with a focused (primary) ion beam under high vacuum. A small fraction of the released surface fragments becomes ionized. Qualitative information of secondary ions from elements, isotopes, and molecular fragments can be acquired in either positive or negative ion mode. These are analyzed based on their mass-to-charge ratio (m/z) by a mass spectrometer, where heavier secondary ions are subject to a larger deviation under the influence of a magnetic field than lighter ions. Ion ejection from the sample surface causes sample charging and the function of an electron gun is to neutralize this charging.

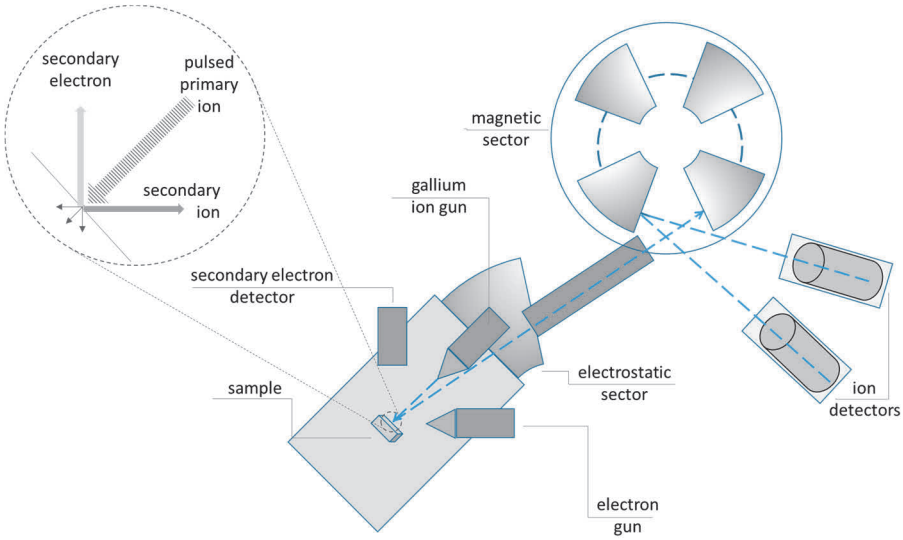

Figure 3.9 *A ToF-SIMS measurement setup.*

A PHI TRIFT II (Physical Electronics Instruments, USA) unit with a pulsed liquid metal ion gun was used to acquire the ToF-SIMS spectra. Positive ion mode spectra were acquired over the mass range of 2-2 000 Da using a Ga^+ primary source with a raster size of 100 × 100 μm^2, a 600 pA aperture current, and a 10 min acquisition time. Sample surface charging was prevented by using a low energy flood gun. Images were collected over a 2 × 2 mm^2 area in non-interlaced mode, i.e., analyses and sputtering are active in different ToF cycles. A challenge when analysing ToF-SIMS spectra of coated papers is that they contain numerous organic compounds originating from the coating formulation, which complicates the identification of the chemical properties directly.

Chapter 4

Results and Discussion

4.1 Printed conductive PEDOT:PSS on natural fibre-based substrates

The CAs of water and PEDOT:PSS water dispersion (Clevios P HC V4, solid content 1.0-1.4 wt.%) for flexographic printing are summarized in Table 4.1. CAs were defined at the time when the oscillations of the droplets had dissipated, but prior to any liquid absorption into the substrate. The CA values were taken after 1 s for water for each sample, whereas for PEDOT:PSS the times varied from 1 s (multilayer coated paper) to 10 s (paperboard) and 60 s (the other samples). Switching of wetting characteristics was observed for TiO2 nanoparticle coated paperboard from superhydrophobic to highly hydrophilic by UVA light irradiation. This behaviour was also observed with water-based PEDOT:PSS ink. The paperboard sample refers to the reference double coated paperboard without nanoparticles.

Table 4.1 *Measured CAs (**Paper I**)*

	Plastic	MLCP	LFS TiO_2	LFS TiO_2+UV	Paperboard
H_2O	75°	50°	153°	7°	74°
PEDOT:PSS	74°	62°	160°	26°	69°

Table 4.2 *Measured sheet resistances with successive prints (**Paper I**)*

	Plastic	MLCP	LFS TiO_2	LFS TiO_2+UV	Paperboard
1st print layer	$> 10^8$	$6.4 \cdot 10^5$	$> 10^8$	$1.2 \cdot 10^6$	$3.6 \cdot 10^6$
2nd print layer	$> 10^8$	$2.0 \cdot 10^5$	$5.3 \cdot 10^6$	$2.9 \cdot 10^5$	$2.7 \cdot 10^5$
3rd print layer	$> 10^8$	$4.0 \cdot 10^4$	$3.3 \cdot 10^5$	$1.0 \cdot 10^5$	$8.0 \cdot 10^4$
4th print layer	$6.2 \cdot 10^5$				

Figure 4.1 presents the scanned images of the flexographic PEDOT:PSS prints. As expected for the TiO_2 nanoparticle coated superhydrophobic surface, the sheet resistance values are higher, as shown in Table 4.2, and print density values are lower due to poor wetting of the surface by the ink and formation of an uneven print layer. In a dynamic printing process, the super-

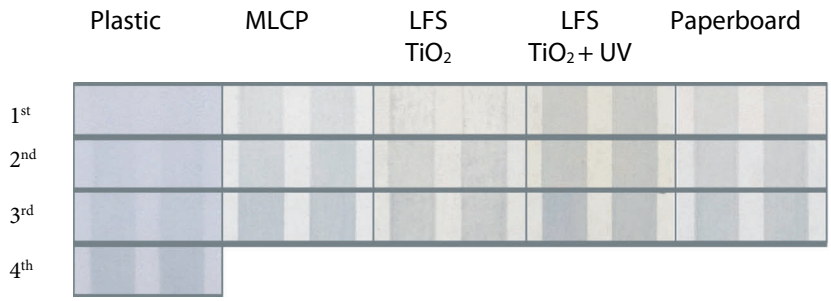

Figure 4.1 *Flexographic PEDOT:PSS prints on different substrates (width of the printed area 7 mm). (**Paper I**)*

hydrophobicity is lost only after several successive print layers. The observed poor ink setting both on plastic film and superhydrophobic LFS TiO_2 correlates well with the observed higher sheet resistance values. The multilayer coated paper contains a barrier layer between the base paper and the thin porous top coating. The barrier layer prevents the PEDOT:PSS ink from penetrating deep into the base paper. Thus, the ink sets at the top resulting in the lowest sheet resistance values.

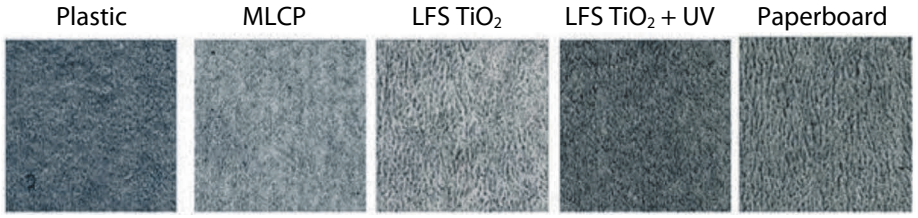

Figure 4.2 *A larger magnification of the flexographic print layer (area 4×4 mm², 3 print layers). (**Paper I**)*

Figure 4.2 shows magnified images of the printed layers. Formation of branched polymer clusters (dark areas) was observed that were especially visible in the paperboard reference. A similar behaviour has been reported with spin-coated PEDOT:PSS thin films (Nardes 2007). This results in anisotropic conductivity values in machine and cross-machine direction. Paper surface roughness was measured by the Parker Print Surf (PPS) device commonly used in paper industry. The plastic film (0.25 μm) and calendered MLCP (0.43 μm) have significantly lower surface PPS roughness than paperboard (1.79 μm). These results are in agreement with previous AFM roughness analysis (Bollström et al. 2009). The paperboard similarly has the highest roughness in

nanoscale (Stepien et al. 2011). The roughness of the paperboard is not significantly changed by the nanoparticle coating (1.71 μm) at the PPS measurement length scale. However, the nanoparticles have previously been shown to increase the nanoscale roughness (Stepien et al. 2011). An optical goniometer study showed that larger PEDOT:PSS droplets tend to form a neck structure due to the polymer concentration increase at the droplet/substrate boundary. PEDOT:PSS droplets initially behave similarly to water. However, as the polymer settles on the surface, the CA grows again with water minimizing its surface energy. For large drops used in the CA measurements, the drying effect is rather slow. In flexography the applied liquid amount is much smaller enhancing the effect and hence, print morphology with similar behaviour may be observed.

Ink setting properties play a crucial role for printed functionality. Finger-like cluster formation shown in Fig. 4.2 is related to the film splitting in the printing nip. The viscous fingering is induced when the PEDOT:PSS ink becomes unevenly split in the printing nip due to local variations of adhesion and wettability. Surface roughness and surface wettability of the substrate may have a considerable effect on the viscous fingering. The high surface roughness and low wettability of surfaces such as LFS TiO_2 nanoparticle coated paperboard makes this phenomenon especially visible. The film splitting hypothesis was confirmed by a rod coating experiment of PEDOT:PSS on the studied substrates. There was no finger formation on these samples with rod coating with lower speed compared to the flexography. The outcome supports the hypothesis that the film splitting in the printing nip is responsible for the viscous fingering.

Figure 4.3 presents the sheet resistance of PEDOT:PSS layers as a function of print density for different print layers. The MLCP has almost a linear decrease of sheet resistance as a function of print density with successive print layers. This result can be related to good ink setting properties in the top coating layer that result in even successive print layers. The plastic film, however, became conductive only after four successive prints.

PEDOT:PSS transfer onto the superhydrophobic LFS TiO_2 nanoparticle coated surface is poor, which leads to high sheet resistance and low print density values. UVA treatment changes the superhydrophobic surface into a highly hydrophilic one. The PEDOT:PSS sets well on such UVA treated surface, as indicated by high print density values. The porosity of the LFS TiO_2 base paperboard is higher than that of the MLCP. This results in a larger PEDOT:PSS transfer onto the UVA treated LFS TiO_2 sample, as observed from

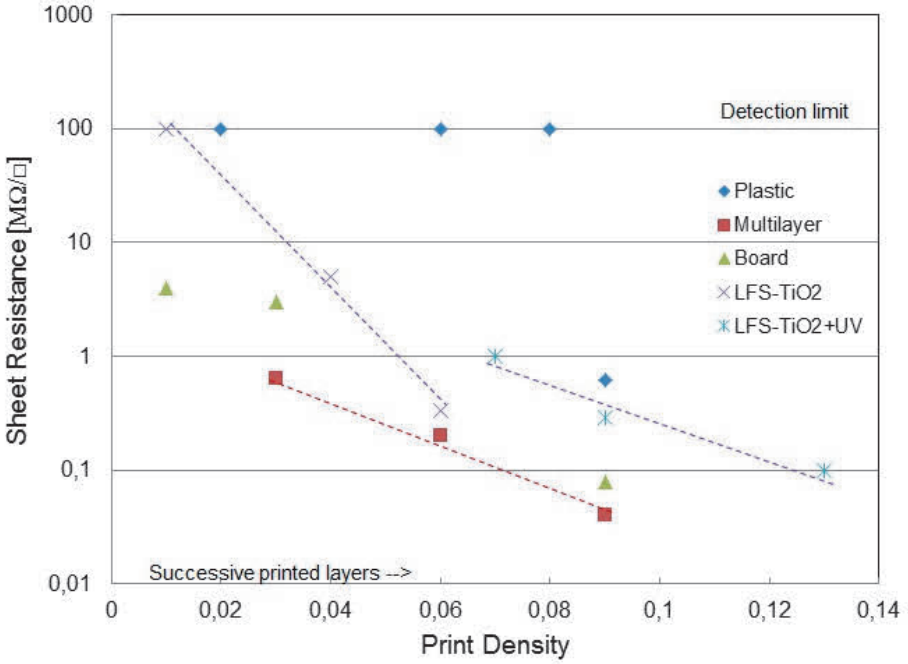

Figure 4.3 *Sheet resistance in PEDOT:PSS as a function of print density for plastic, multilayer, and LFS paperboard (reference, LFS-TiO_2, and LFS TiO_2+UVA treated paperboard).* (***Paper I***)

the higher print density values compared to the MLCP. However, the sheet resistance values are higher for the former. It can be concluded that PEDOT:PSS absorbed deep into the porous paperboard does not significantly contribute to conductivity. This shows well the importance of controlled printability for printed functionality. The penetration of PEDOT:PSS into the LFS TiO_2 base paperboard can be controlled by adjusting the surface wettability by UV irradiation. The optimal printing speed for the IGT printer for PEDOT: PSS was > 1.0 m/s for adequate reproduction and minimization of the finger formation. From a practical point-of-view it is beneficial to reduce the number of successive printing cycles by optimizing the used anilox roll that can increase the homogeneity of the print and produce conducting layers even with a single print.

4.2 Effect of polyelectrolytes on PEDOT:PSS conductivity

Polyelectrolytes can be described as salts chained to each other. Polyelectrolytes are added during the papermaking process at the wet end of a paper machine to improve retention of mineral pigment fillers embedded into the fibre matrix of the pulp as well as retention of starch, gum, or rosin sizing during the formation of the base paper (Alén 2007). In mineral pigment coating formulations the polyelectrolytes act as dispersing agents fully covering the pigment particle surface (Paltakari 2009). Therefore, printed conductive layers on paper substrate are exposed to potential electrolytes at the ink-paper interface. However, it is worth emphasizing that the polyelectrolyte concentrations used in **Paper II** on glass substrates are significantly higher than those actually found in the coated paper surfaces. The current study pinpoints important issues that need to be taken into account when designing printed electronics and functionality on economically, ecologically, and environmentally sustainable pigment coated paper substrates.

While the electrical performance of PEDOT:PSS is well-known (Löwenich 2014), the effect of anionic and cationic polyelectrolytes on the electrical performance has not been thoroughly investigated. This is of interest for paper-based electronics since polyelectrolytes, such as PA and pDADMAC, are commonly used as dispersants for paper coating pigments. The sheet resistance of spin-coated PEDOT:PSS is in the kΩ/□ range, whereas the measured sheet resistance of cationic pDADMAC was 1-2 orders of magnitude higher in the MΩ/□ range. The anionic PA behaves like an isolator with sheet resistance values in the GΩ/□ region. Both pDADMAC and PA are inherently hygroscopic (Wong et al. 2004) and coatings of them are thus prone to dimensional instability, especially at high relative humidity conditions.

The PEDOT:PSS polymer complex consists of cationic, conductive, and hydrophobic PEDOT groups adsorbed on anionic PSS polyelectrolyte chains. The strong PSS polyelectrolyte is fully charged and dissociates completely in water. The presence of PA makes it easier for PEDOT to blend with water, forming PEDOT:PSS water dispersion particles with a water content of 90-95 wt.%. The hydrophobic PEDOT groups are pushed into the centre of the dispersion particle surrounded by anionic PSS and water. These colloidal particles are the building blocks of the conductive PEDOT:PSS films and coatings (Mochizuki et al. 2012).

Structure, packing density, and conductivity of the PEDOT:PSS film is governed by several factors including the used transfer method, carrier liquid

composition, drying method, and drying time. In spin-coating, the quaternary structure of PEDOT:PSS can further be segregated by the centrifugal forces into lentil-like PEDOT-rich clusters embedded between very thin PSS lamellas. Some PSS residue is transported along with the evaporating water onto the surface of the conductive polymer (Nardes 2007, Fabretto et al. 2008).

Figure 4.4 presents sheet resistance and print density of PEDOT:PSS on spin-coated PA (a) and pDADMAC (b) with a varying polyelectrolyte concentration. PA is a strong polyelectrolyte that blends effectively with dispersed PEDOT:PSS in water. Together they form a smeared coating supporting non-uniform film coverage with strong local colour shifts. These non-uniformities caused a large sample to sample variation. Hence, the print density and sheet resistance values display significant standard deviations, especially with the largest PA concentration. These samples lacked consistency in print density and resulted in a larger sheet resistance than the PEDOT:PSS single layer reference. The print density on the reference glass slide was 0.09-0.10 units, and is included in all the reported print densities.

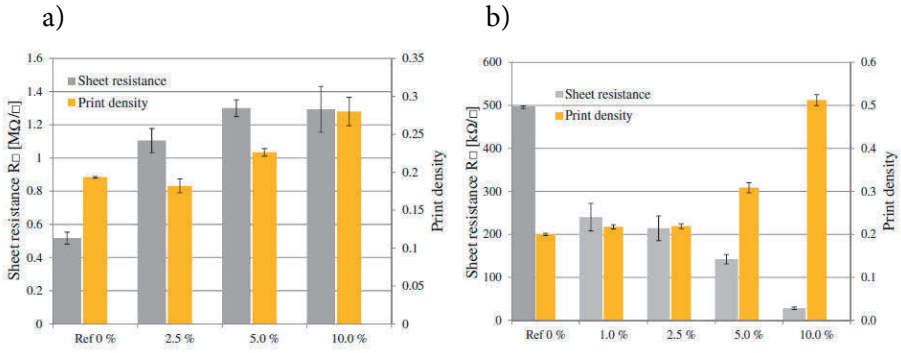

Figure 4.4 *Sheet resistance and print density values of spin-coated PEDOT:PSS on PA (a) and pDADMAC (b) on coated glass as a function of the added polyelectrolyte. (**Paper II**)*

Spin-coated PEDOT:PSS coating set better on pDADMAC (Fig. 4.4b) films than on PA samples. PEDOT:PSS and pDADMAC are oppositely charged and the formation of darker PEDOT:PSS coatings on higher pDADMAC concentration was observed. The sheet resistance was lower for pDADMAC/PEDOT:PSS bilayers in comparison to the single layer PEDOT:PSS reference. In addition, the pDADMAC/PEDOT:PSS bilayers displayed only marginal defects or local variations, which translates into consistent values and

narrow standard deviations. Contrary to these results, addition of pDADMAC into the bulk PEDOT:PSS water dispersion makes the dispersion particles collapse and separate. At the pDADMAC/PEDOT:PSS interface, this problem was avoided by keeping the pDADMAC coating exposure times to PEDOT:PSS dispersion below 20 s.

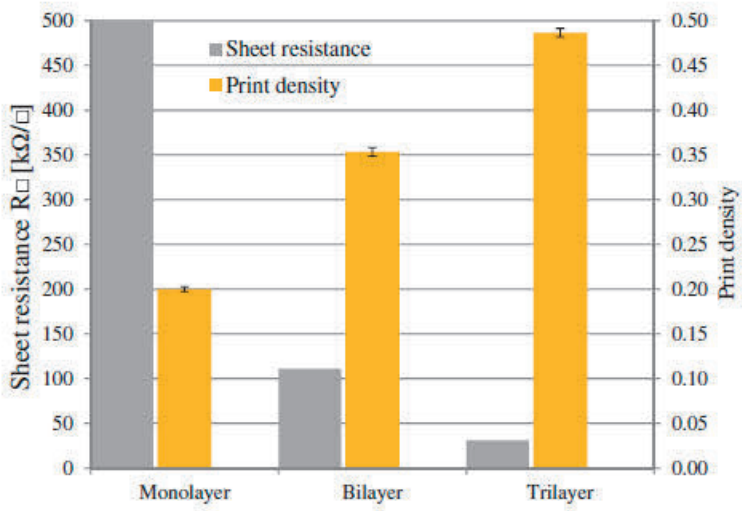

Figure 4.5 *Sheet resistance and print density values of spin-coated layer-by-layer PEDOT:PSS samples. (**Paper II**)*

A layer-by-layer deposition of PEDOT:PSS was conducted in the absence of polyelectrolytes. Multiple layers were expected to produce a thicker PEDOT:PSS coating combined with a high print density (i.e. dark colour) and a low sheet resistance. As expected, sequential spin-coated PEDOT:PSS shown in Fig. 4.5 can significantly lower the sheet resistance that correlates well with the print density increase. The sequential PEDOT:PSS bi- and trilayer structures are in good agreement with the sheet resistance and print density values of the pDADMAC/PEDOT:PSS bilayers shown in Fig. 4.4b with 5 and 10 wt. % pDADMAC concentration, respectively.

SEM was used to determine the thickness and structure of the spin-coated samples. The PEDOT:PSS single layer in Fig. 4.6 (a) has a total thickness of approximately 90 nm. The diameters of individual dispersion particles range from 45 to 60 nm, thus, forming a coating that consists of two layers of dispersion particles.

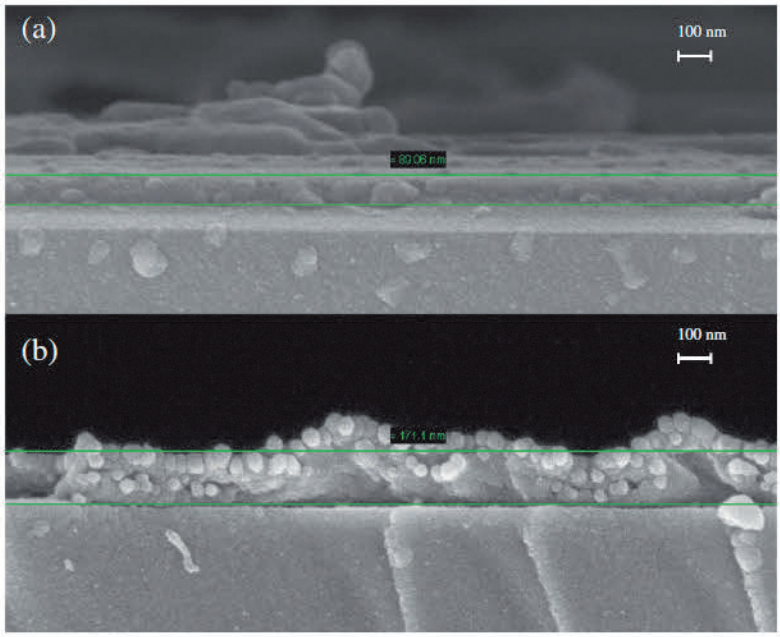

Figure 4.6 *SEM images of nitrogen freeze-fractured, spin-coated PEDOT:PSS layers on glass showing dispersion particles that remain intact on the surface despite the spin-coating. The film thickness of PEDOT:PSS is approximately 90 nm. Image magnification: 50 000×. (**Paper II**)*

Table 4.3 *Thicknesses of single layer pDADMAC and pDADMAC/ PEDOT:PSS bilayers. (**Paper II**)*

Single layer sample	d[nm]	Bilayer sample	d[nm]
1.0 wt.% pDADMAC	30-50	1.0 wt.% pDADMAC/PEDOT:PSS	110
2.5 wt.% pDADMAC	120-130	2.5 wt.% pDADMAC/PEDOT:PSS	210-250
5.0 wt.% pDADMAC	300-310	5.0 wt.% pDADMAC/PEDOT:PSS	230-260
10.0 wt.% pDADMAC	710-750	10.0 wt.% pDADMAC/PEDOT:PSS	360

Thickness data of pDADMAC and pDADMAC/PEDOT:PSS samples are presented in Table 4.3. The pDADMAC coating thickness increases with increased polyelectrolyte concentrations from 33 nm at 1 wt.% pDADMAC to 748 nm at 10 wt.% pDADMAC. The layer thickness increase does not follow the concentration linearly due to higher viscosities with increased polyelectrolyte concentration. This is caused by higher persistence against deformation induced by the centrifugal and compressive forces during the spin-coating. At higher polyelectrolyte concentrations of 5 and 10 wt.%, the

single layer pDADMAC exceeds the total thickness of bilayer pDADMAC/PEDOT:PSS samples caused by saturated PEDOT:PSS absorption.

Figure 4.7 shows that the quaternary structure of PEDOT:PSS is retained in all the bilayer samples on pDADMAC, which is not self-evident. Higher pDADMAC concentrations create a stronger attraction for PEDOT:PSS dispersion particles followed by a thicker adsorption layer. A diffuse region is formed in the interface between the pDADMAC and the PEDOT:PSS layer. The PEDOT:PSS water dispersion particles blend together with the pDADMAC coating, which is a typical spin-coating phenomenon. At higher pDADMAC concentrations of 5 and 10 wt.% the bilayer fabrication process becomes increasingly difficult. Some thinning of the bilayer samples was observed, but the exact mechanism behind this is unclear.

PA and PEDOT:PSS blend easily. However, when an isolator is introduced into the PEDOT:PSS, the outcome will have a lower conductivity compared to a single layer PEDOT:PSS reference. Thus, anionic PA caused a considerable sheet resistance increase, whereas PEDOT:PSS on pDADMAC showed an increased conductivity.

Figure 4.8 proposes a hypothesis and a step-by-step description of the PEDOT:PSS interaction on top of pDADMAC. The initial PEDOT:PSS exposure (Fig. 4.8a) is followed by an adherence to the polyelectrolyte surface. In the vicinity of the pDADMAC/PEDOT:PSS –interface, the bulk PEDOT:PSS water dispersion phase becomes destabilized by strong attraction induced by the oppositely charged pDADMAC. A saturated PEDOT:PSS adsorption layer is formed at the liquid-solid interface that is governed by the dry content of pDADMAC (Fig. 4.8b and c). Once the distance increases beyond the threshold to destabilize the dispersion, the adsorption ceases and the PEDOT:PSS layer reaches its maximum thickness. According to Fig. 4.7, the quaternary structure of PEDOT:PSS is retained during the spin-coating. When exposed to PEDOT:PSS with a molecular weight around 100 kDa, the pDADMAC underlay provides an extended time window by preventing it from softening up, blending and quickly passing through the PEDOT:PSS adsorption layer into the bulk phase. Finally, the PEDOT:PSS adsorption layer structure is partly or completely destabilized when exposed to prolonged deposition times (>60 s) prior to the spin-coating, as shown in Fig. 4.8d. The difficulties experienced during the sample preparation also suggest that the saturated PEDOT:PSS adsorption layer is very prone to defects disturbing the quaternary layer structure that is caused by locally applied external pressure

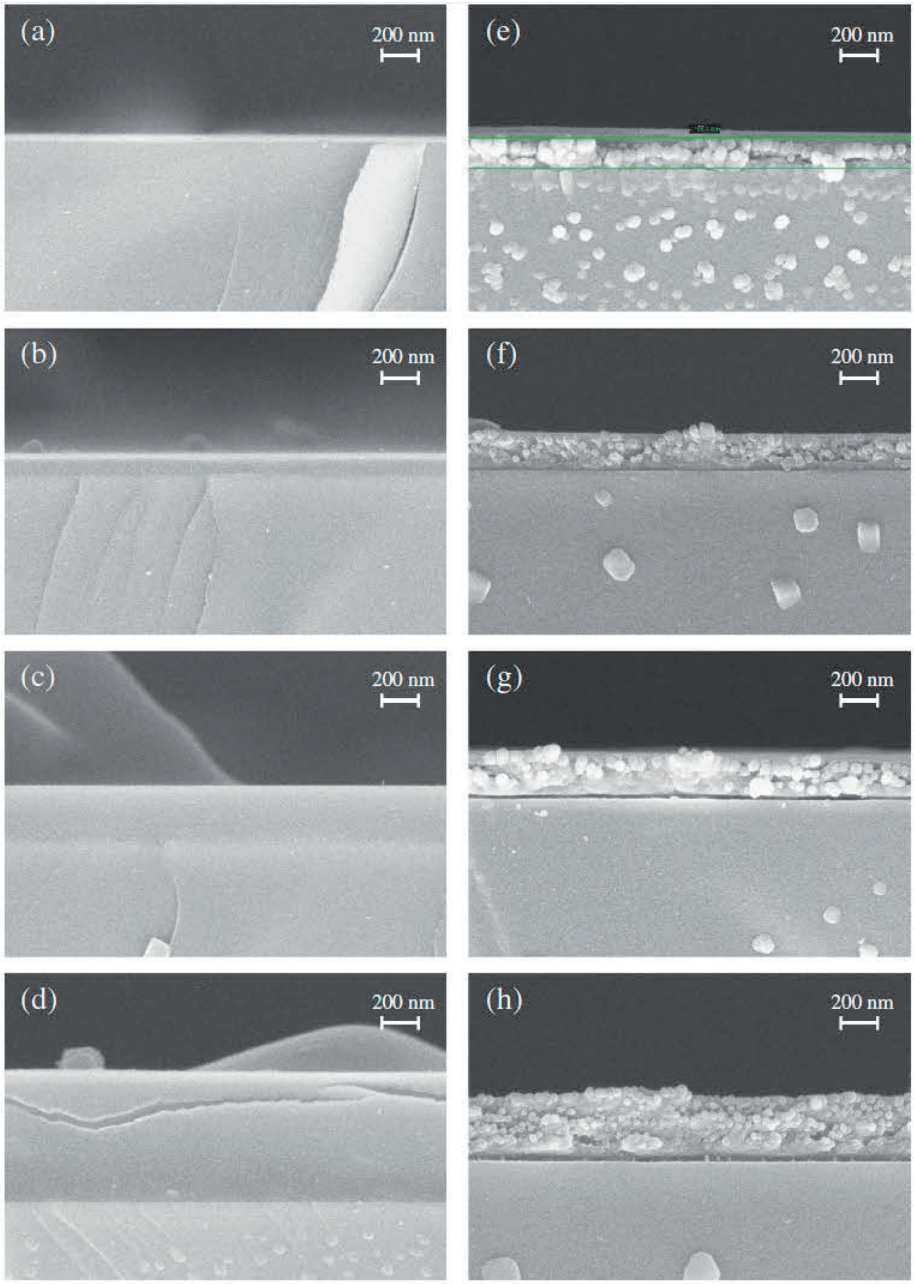

Figure 4.7 *(a–d): 1.0 wt.%, 2.5 wt.%, 5.0 wt.%, and 10.0 wt.% single layer pDADMAC, respectively. (e–h): spin-coated pDADMAC/PEDOT:PSS bi-layers with identical concentration as in (a–d). Image magnification: 50,000×. (**Paper II**)*

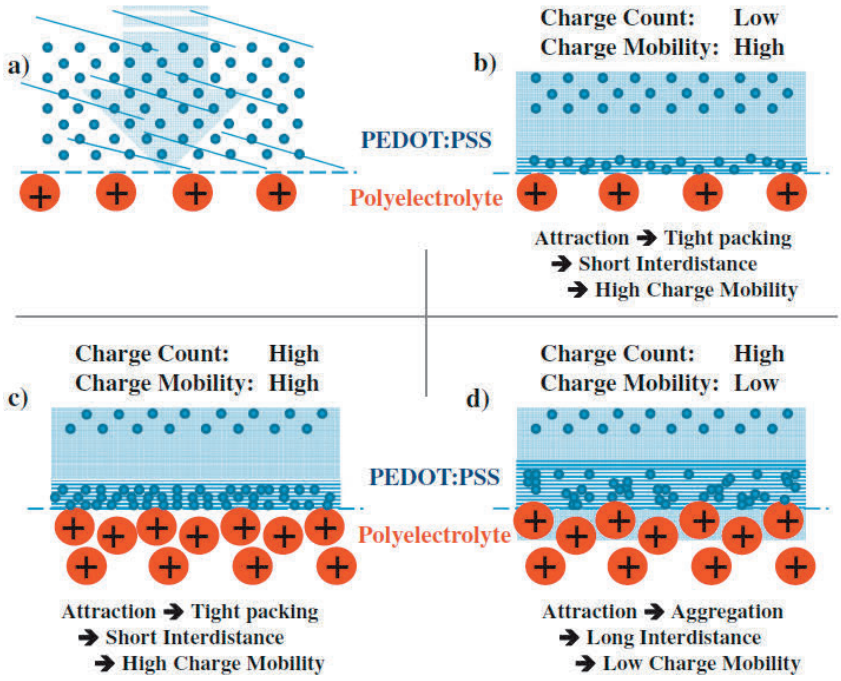

Figure 4.8 *Deposition of PEDOT:PSS on cationic pDADMAC.* ***(Paper II)***

during the PEDOT:PSS deposition. This does not have a significant impact on the print density, but the electrical performance can vary considerably. This is worth emphasizing especially when dealing with contact printing methods.

To summarize, based on the SEM cross-section image data of pDADMAC/PEDOT:PSS bilayers, there is a strong dependency between the PEDOT:PSS coating thickness and print density. Furthermore, the pDADMAC solid content has a strong impact on the adsorbed PEDOT:PSS coating thickness. The amount of PEDOT:PSS adsorbed on 5.0 and 10.0 wt.% pDADMAC resembles the amount of two or three times sequentially coated PEDOT:PSS layers. Hence, the saturated PEDOT:PSS adsorption layer is mainly responsible for the electrical conductivity in the pDADMAC/PEDOT:PSS bilayers.

4.3 Conductivity of PEDOT:PSS on NFC-G

The PEDOT:PSS coating interaction was studied with NFC films which are a promising biodegradable substitute to packaging and display materials made of plastic in the future. The main objective was to understand the effect of

glycerol in the NFC film layer for potential enhancement of PEDOT:PSS conductivity.

In general, the conductivity of PEDOT:PSS can be increased by annealing, increased film thickness, or introduction of a secondary dopant. Polyols form a common group of secondary dopants. Glycerol was selected as a secondary dopant based on its multiple functions in material blends. In this particular case, the glycerol is also a plasticizer adding flexibility to the otherwise brittle NFC film. The conductivity enhancement provided by the presence of glycerol can turn the NFC into an active functional coating alongside serving as a semi-transparent substrate for the PEDOT:PSS coatings.

PEDOT:PSS was applied on either drop cast or spin-coated NFC films at various solid contents. The NFC-G films were left to dry before the PEDOT:PSS spin-coating. Conductivity measurements require a very high sample-to-sample reproducibility that is achieved through a uniform and smooth film quality. Such sample characteristics also allow reliable sessile drop wetting studies. The semi-transparent and optically clear samples, including substrate and all coating layer components (glass substrate, PEDOT:PSS, NFC, and glycerol), resulted in a semi-transparent structure suitable for UV-VIS transmission studies.

The effect of glycerol on NFC-G conductivity was studied both at a constant glycerol concentration with varying NFC concentration (Fig. 4.9a) and at a constant NFC concentration with varying glycerol concentration (Fig. 4.9b). In Fig. 4.9 (a), PEDOT:PSS was spin-coated on top of drop cast NFC-G which had varying NFC concentration and a constant glycerol level (5.0 wt.%). This resulted in sheet resistance levels of three orders of magnitude lower than the reference PEDOT:PSS. The sample annealing temperature ranged from 60 to 130°C. With increasing temperature above 80°C, the PEDOT:PSS conductivity becomes increasingly consistent and reproducible.

Addition of glycerol into the PEDOT:PSS enables a morphological rearrangement of the PEDOT and PSS species increasing the conductivity. It is sufficient for secondary dopants to evaporate or pass through the PEDOT:PSS layer leaving without a trace and still make the PEDOT:PSS more conductive (Friedel et al. 2009, Friedel et al. 2011).

PEDOT:PSS behaved nearly identically on drop cast 0.05 and 0.1 wt.% NFC-G at a constant 5 wt.% of glycerol. A further increase of NFC concentration to 0.2 wt.% resulted in a sheet resistance increase. The concentration has an impact on the coating viscosity, which in turn produces a thicker coating layer. Absorption and blending at the NFC-G/PEDOT:PSS

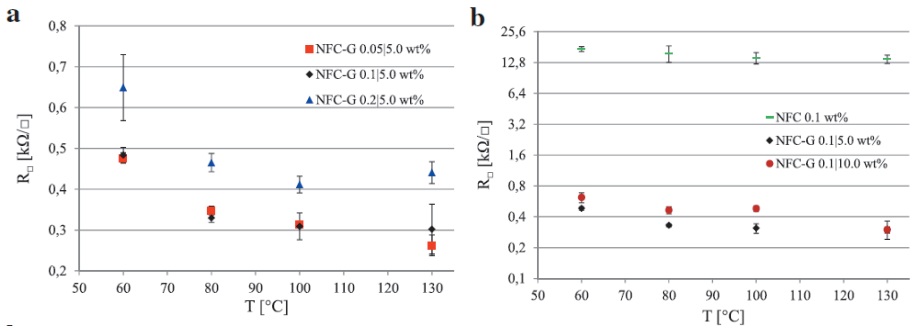

Figure 4.9 *PEDOT on drop cast NFC-G. (**Paper III**)*

interface is thus weakened due to the increased viscosity and reduced deformability of the NFC-G coating. Annealing may create mechanical strain due to non-uniform drying of the NFC-G coating. This may cause a higher sheet resistance due to cracking and lowered film quality in the PEDOT:PSS layer. It is worth mentioning that despite these possible defects, the sheet resistance of the PEDOT:PSS on drop cast NFC-G is well below the PEDOT:PSS reference on glass.

PEDOT:PSS on drop cast NFC-G at a constant NFC concentration with varying glycerol levels provided improved conductivity in all three cases, as shown in Fig. 4.9 (b). The NFC film with no added glycerol resulted in a drop of the PEDOT:PSS sheet resistance from the reference level of 550 kΩ/□by a factor of 30 down to 18 kΩ/□ The improved conductivity originates from water that is left in the NFC coating evaporating through and rearranging the PEDOT:PSS layer (Friedel et al. 2009, Friedel et al. 2011).

The lowest sheet resistance values were achieved at 5 wt.% of glycerol. An increase from 5 wt.% to 10 wt.% did not bring any further improvement. The mechanical properties start to fail at higher glycerol levels followed by a disintegration during the spin-coating of PEDOT:PSS. While pure NFC coating does enhance the PEDOT:PSS conductivity, a considerable sheet resistance drop is achieved only with the involvement of glycerol.

The drop cast method is a time consuming process, where the sample drying is defined by the quantity and evaporation rate of the solvent under ambient or controlled conditions. The outcome of drop casting is a relatively thick layer compared to the spin-coated layers. Exposure to compression and quick drying produce thinner films during the spin-coating. In the case of spin-coated NFC, the denser film texture also has increased barrier characteristics. Spin-coating reduces NFC-G film processing times to a few

minutes from 24h that it typically takes for the drop cast samples to dry at ambient conditions.

Figure 4.10 presents the sheet resistance of PEDOT:PSS on spin-coated NFC-G. Samples were differentiated by varying the NFC concentration and/or the spinning rate. On 0.1/5.0 wt.% NFC-G, the PEDOT:PSS produced an identical output to the PEDOT:PSS deposited directly on a glass. At annealing temperatures of 60 and 80°C, the pronounced standard deviations of the results are due to the unstable nature of PEDOT:PSS in this temperature range. This is considered as an indication of lack of interaction between the PEDOT:PSS and the NFC-G layer during the spin-coating or the annealing stage.

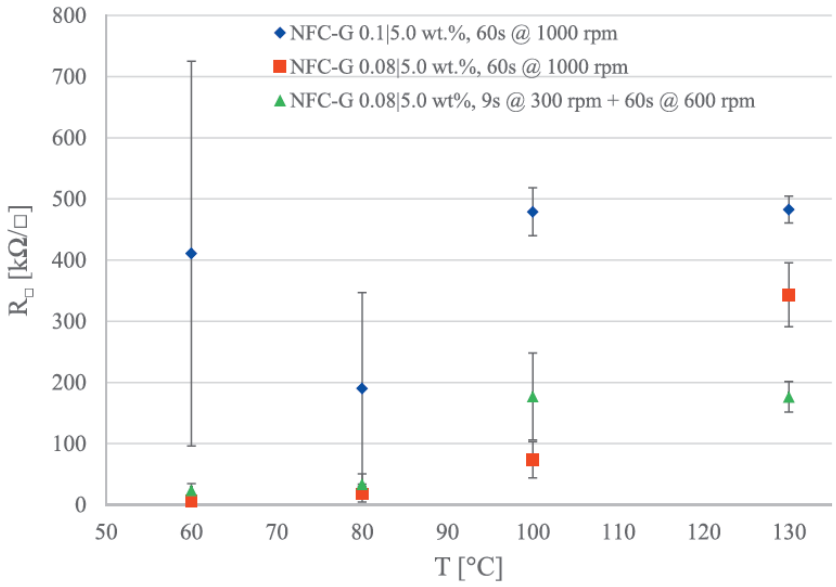

Figure 4.10 *PEDOT on spin-coated NFC-G.* ***(Paper III)***

A concentration drop from 0.1 to 0.08% wt.% made the NFC-G mixture less viscous producing thinner films at a constant spinning rate of 1000 rpm. A considerable drop and stabilization in sheet resistance was observed. This resulted from PEDOT:PSS interaction with glycerol. A further lowering of the spinning rate down to 600 rpm including an initialization interval of 300 rpm, allowed more NFC-G to remain on the substrate surface. Hence, a thicker film was formed. At lower temperatures, sheet resistance values stayed at the same level, whereas at 100 and 130°C the sheet resistance values were slightly below

200 kΩ/□. This was clearly on a lower level than the 550 kΩ/□ of the PEDOT:PSS reference on glass.

At the higher NFC concentration of 0.1 wt.%, a denser layer was formed that provided barrier properties - preventing glycerol from leaving the NFC-G layer to interact with the PEDOT:PSS. At 0.08 wt.% of NFC, the glycerol component may migrate from the less dense NFC-G layer and mix with the PEDOT:PSS during the spin-coating and annealing stage. Therefore, customized, spin-coated NFC-G coating can either become a barrier (0.1 wt.%) or regulator (0.08 wt.%) that can tap glycerol and water into the PEDOT:PSS layer.

One of the objectives of the NFC-G model system on a glass substrate was to retain the semi-transparent characteristics of the self-supporting NFC-G film. A smooth NFC-G coating on a rigid glass substrate allows spin-coating and formation of a good quality PEDOT:PSS coating. The results in Figs. 4.9 and 4.10 indicate that the samples meet the requirements for electrical and optical characterization.

WCAs on different NFC-G/PEDOT:PSS coatings are shown in Fig. 4.11. All PEDOT:PSS coated samples were annealed at 130°C and stored for 24h at RH 50% prior to CA characterization. Spin-coated and drop cast NFC-G formed strongly hydrophilic coatings. The drop cast NFC-G showed strong water absorption in the time interval from 15 to 40 s causing swelling and deformation. Residual markings on the spin-coated NFC-G coating after the finished CA experiment suggest very limited water absorption. CA measurements were also performed on glycerol coated glass. Highly hydrophilic surface was observed but these results were not included, as water droplets formed irregular, noncircular wetting patterns on the surface and thus did not allow a reliable conventional interpretation of CA data based on symmetrical wetting patterns.

The PEDOT:PSS samples were less hydrophilic in comparison to the uncoated NFC-G samples. PEDOT:PSS on spin-coated NFC-G produced an identical outcome compared to the reference PEDOT:PSS on glass. PEDOT:PSS samples on drop cast NFC-G had WCAs approximately 15° above the reference. However, all the involved components NFC, glycerol and PEDOT:PSS are hydrophilic when measured on their own. Therefore, the origin of the CA rise may be due to surface deformation and roughness effects. Annealing, in general, has a smoothening effect on the PEDOT:PSS coating. Deformations in the NFC-G coating layer occur when water originating from the PEDOT:PSS is absorbed and evaporates through the pores and pinholes

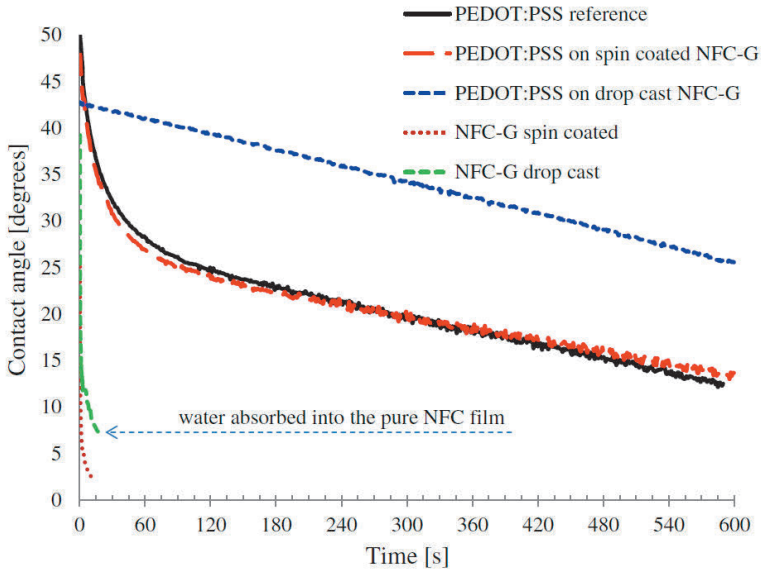

Figure 4.11 *CA data of pure and PEDOT:PSS coated NFC-G films. (**Paper III**)*

into the PEDOT:PSS. Nevertheless, despite its rough surface, the PEDOT:PSS coating retains its barrier properties, as shown in Fig. 4.11.

Figure 4.12 presents the optical transmission of PEDOT:PSS on drop cast or spin-coated NFC-G. The spin-coated NFC-G overlaps with the reference PEDOT:PSS on glass with a range from 94% to 84% transmission rate across the measured spectral range. The maximum transmission is located in the blue region. Both these sample categories retain their light blue colour shade. The colourless NFC-G coating seems to have little or no impact on the transmission.

PEDOT:PSS on drop cast NFC-G resulted in one to eight units lower transmission across the whole spectral range. This is considered to be of little harm in comparison to the conductivity increase of three orders of magnitude. The PEDOT:PSS becomes absorbed into the NFC-G coating layer. This creates a dark blue colour shade and thus, an additional drop in transmission. PEDOT:PSS consists of more than 95 wt.% water that can easily become absorbed by the NFC-G coating, as shown in Fig. 4.11. All samples annealed between 60°C and 130°C behaved optically equally. Finally, the spin-coated samples remained reproducible within one percentage point, whereas drop cast samples were within three percentage points.

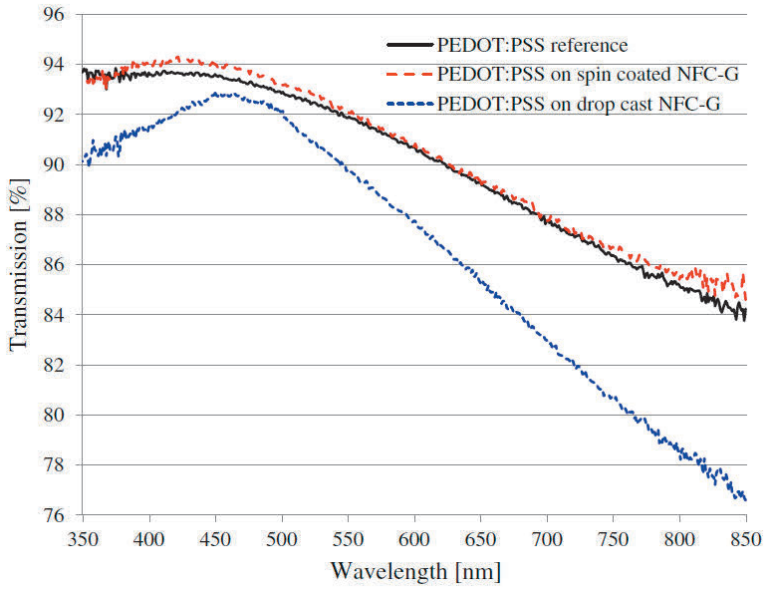

Figure 4.12 *Optical transmission of PEDOT:PSS on NFC. (**Paper III**)*

4.4 Permanent planar fluidic channels on TiO_2 nanoparticle coated paperboard

The adhesion of LFS deposited nanoparticles on a surface is predominantly controlled by van der Waals long range forces, i.e. the particles are loosely bound to the surface. Earlier work has shown that the UVA light facilitated wettability conversion is not permanent on the TiO_2 nanoparticle coated paperboard, i.e. the illuminated area returns to the initial superhydrophobic level in storage, and the recovery can be accelerated by heat (Teisala et al. 2013). However, there are not always UVA light sources available for converting TiO_2 nanoparticle samples to highly hydrophilic. Therefore, in **Paper IV**, a more permanent TiO_2 nanoparticle wettability conversion approach was studied. To make the channel structures more permanent, a water treatment step with first stage wetting was added, as depicted in Fig. 3.4 (p. 29).

One and two mm wide channel structures were created by a UVA illuminated area through a mask on a TiO_2 nanoparticle coated paperboard, as displayed in Fig. 4.13(a) without and (b) with the first stage wetting step. In Fig 4.13(a), the first stage non-wetted channel is exposed to red coloured water (Amaranth dye) for a better visualization and contrast. No channel structure becomes visible, as the actions of UVA illumination followed by heat treatment cancel each other, and thus channel structure is lost with surface recovery to

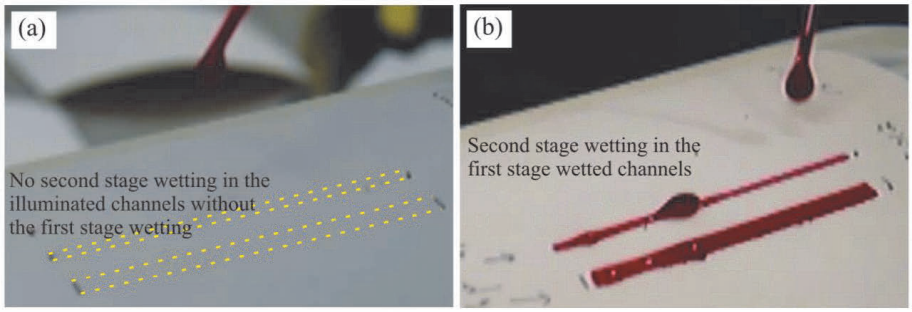

Figure 4.13 *Images of wetting behaviour of samples without (a) and with (b) the first stage wetting in 1 and 2 mm wide channel structures that are exposed to red colour stained water. The illuminated channels in (a) indicated by yellow dotted lines convert back to superhydrophobic by the heat treatment whereby they are not wetted by the coloured water. (**Paper IV**)*

superhydrophobic. In Fig. 4.13(b), a clear second stage wetting takes place in the first stage wetted channel structures.

WCAs of the TiO_2 nanoparticle coated paperboard are summarized in Table 4.4: as prepared (CA ~ 160°), followed by UVA illumination (CA ~ 5°), heat treated first stage wetted channel (CA ~ 110°), and followed by a repeated, secondary post-UVA illumination (CA ~ 65°). As reported earlier (Stepien et al. 2012), heat treatment of the sample recovers the initial superhydrophobicity.

Table 4.4 *WCAs of the channel areas. (**Paper IV**)*

Sample	CA [°]
Reference-based paperboard	78
Initial TiO_2 NP surface	160
UVA illuminated channel	5
Heat treated first stage wetted channel (0s → 60s)	110 → 100
Heat treated first stage wetted channel exposed to post UVA Illumination (0s → 60s)	102 → 65

However, after the heat treatment, the WCA of the first stage wetted channel is close to 110° which is significantly lower than the initial superhydrophobic value. Therefore, the wettability of the channel structure is permanently increased compared to the case without the first stage wetting. Furthermore, the initial WCA will drop by 10° within 60 seconds from 110° to 100°. In the

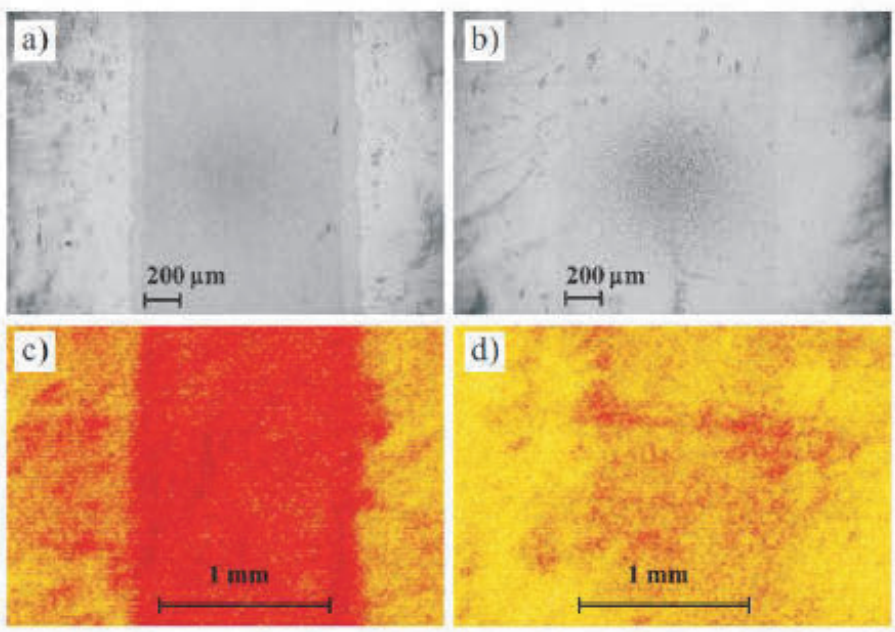

Figure 4.14 *FE-SEM (a, b) and ToF-SIMS images of total ion counts in positive ion mode (c, d) of the channel structure with (left) and without (right) the first stage wetting in a 1 mm wide channel structure. (**Paper IV**)*

same timeframe of 60 s the channel area WCA drops by additional 37° from 102° to 65° with a repeated UVA illumination. It is reasonable to assume that the number of TiO_2 nanoparticles in the channel structure is reduced during the first wetting stage, as no extreme WCAs are reached after the secondary UVA treatment. The reduction in nanoparticle number hypothesis was confirmed by electron microscopy in both cases.

Microscopy results in Fig. 4.14 show the FE-SEM and ToF-SIMS total ion count images of the UVA and annealed channels with and without the first stage wetting. A comparison between the left-hand side and the right-hand side image shows a significant difference between the first stage wetted channel compared to the non-wetted channel structure. The channel structure width corresponds well to the UVA photomask exposure area with a width of 1 mm. The nanoparticles on the highly hydrophilic channel area are transported away along the moving liquid contact line and pushed to the edges similar to the coffee stain effect (Deegan et al. 1997) or absorbed into the base paperboard mineral pigment coating during the first wetting stage.

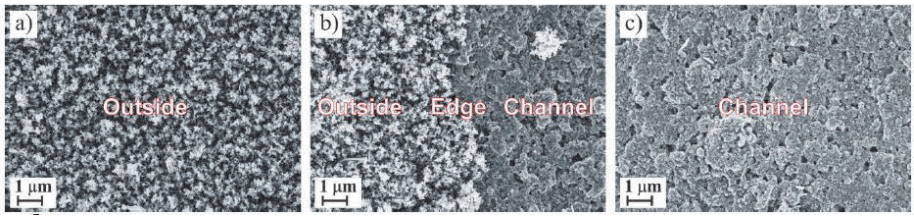

Figure 4.15 *FE-SEM images of outside, edge, and channel areas of the first stage wetted TiO2 nanoparticle coated surface. A rosette-like structure of TiO2 nanoparticles fully covering the surface is shown on (a) whereas a typical base paperboard mineral pigment coating structure is clearly visible in the first stage wetted channel with the reduction of TiO2 nanoparticles, as seen in (c). (**Paper IV**)*

The surface morphology of the channel and edge region was studied in more detail using an FE-SEM, as shown in Fig. 4.15. The area outside the channel (no UVA exposure, oven heat treatment only) has a typical morphology of the LFS deposited TiO_2 nanoparticles, as observed in earlier work (Stepien et al. 2013). A significant decrease in the number of nanoparticles is clearly visible in the channel area, as shown in Fig. 4.15c. A distinct boundary can be observed in the edge area between the channel and non-wetted area in Fig. 4.15b.

FE-SEM and ToF-SIMS observations were confirmed by the XPS elemental composition results displayed in Table 4.5. The amount of titanium is reduced as a direct consequence of the first stage wetting that supports the findings from the FE-SEM images. Furthermore, the surrounding areas, which are only exposed to heat, show similar values.

Table 4.5 *Relative amounts of elements in different elements. (**Paper IV**)*

Sample	C 1s	O 1s	Ti 2p
First stage wetted / channel	55.1	35.4	9.1
First stage wetted / outside	49.0	38.8	12.2
Non-wetted / channel	51.4	36.8	11.0
Non-wetted / outside	48.9	38.5	12.6

The small decrease in the amount of titanium in the non-first stage wetted channel area (UVA + oven treatment) correlates with the increased amount of carbon: during the heat treatment volatile organic components are evaporated from the base pigment paperboard coating that can adhere on top of the TiO_2

nanoparticles, as shown also in previous studies. A more significant reduction of titanium is observed after the water treatment in the first stage wetted channel area in agreement with previous work (Stepien et al. 2012, Stepien et al. 2013).

Figure 4.16 displays the high resolution ToF-SIMS spectra with two different *m/z* ranges that correspond to fragments of Ca and C_3H_4 peaks (39.8-40.2), and OC_2H_3 and C_3H_7 (42.8-43.2). A large Ca-ion peak is only visible in the first stage wetted channel. The weakly acidic deionized water (pH 5.6) causes the carbonate pigments in the paperboard coating to dissolve. Hence, as seen from the high resolution FE-SEM image in Fig 4.15, the base paperboard $CaCO_3$ particles in the pigment coating are partially dissolved. Previous studies show that the LFS deposited TiO_2 nanoparticles are covered with a carbonaceous layer (Teisala et al. 2013). This hydrocarbon layer originates

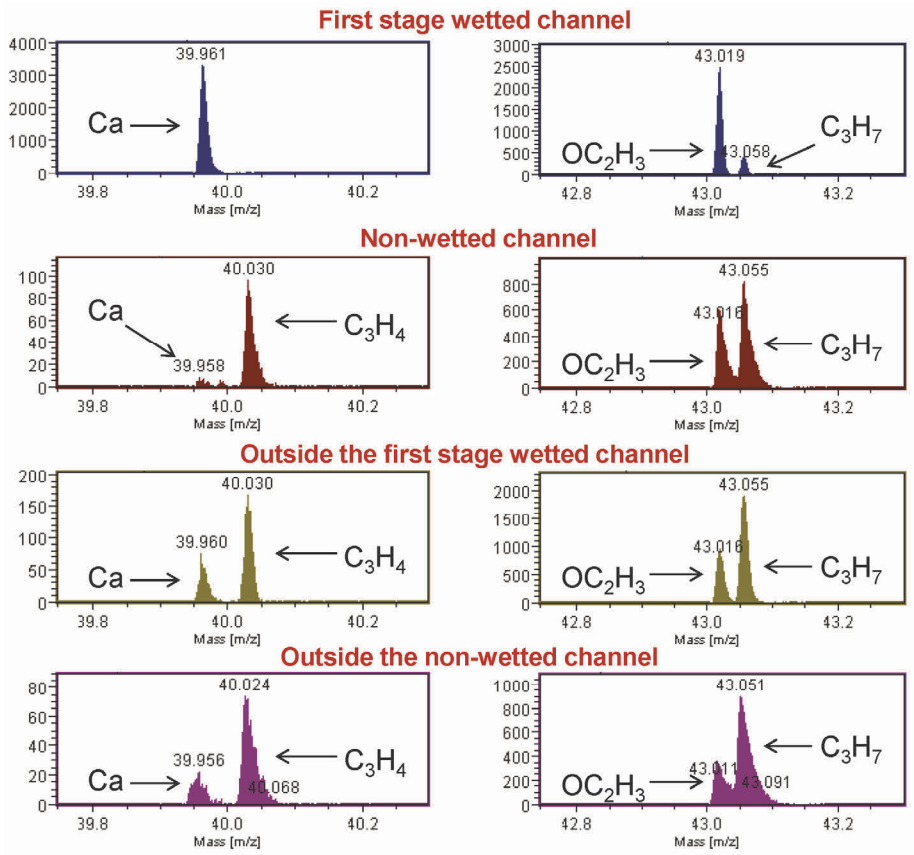

Figure 4.16 *High resolution ToF-SIMS spectra of peaks 40 and 43 of the different samples. (**Paper IV**)*

from the combustion of volatile organic compounds released from the organic binder material during the flame deposition. It is also visible in Fig. 4.16, the C_3H_4 peaks being absent in the first stage wetted channel at 40.03 due to the reduction of TiO_2 nanoparticles from the channel. The hydrocarbon peaks in the vicinity of m/z = 43 are also visible in the high resolution ToF-SIMS spectra in Fig. 4.16.

There is also a significant increase in the polar hydrocarbon peak of OC_2H_3, whereas the non-polar hydrocarbon peak of C_3H_7 is smaller than in the other spectra. Thus, the first stage wetted channel becomes less hydrophobic than the non-wetted channel. The recorded peaks of 54, 55, 56, and 57 confirm that the coating colour components are only visible in the first stage wetted channel. It is worth emphasizing that only the outermost molecular layers of the surface (1-2 nm in depth) are characterized by the ToF-SIMS. In the case of the non-wetted channel, the base paperboard is located well below the detection range. Hence, the ToF-SIMS signal mainly originates from the porous TiO_2 nanoparticle coating layer. In the first stage wetted channel, the base paperboard becomes exposed and is within the detection range. This is supported by the FE-SEM images in Fig. 4.16.

The normalized relative intensities of the ToF-SIMS spectra from the channel area are shown in Fig. 4.17. Removal of the TiO_2 nanoparticles caused by the first stage wetting translates into smaller intensities for the peaks m/z = 46 Da (Ti), 48 Da (Ti), 64 Da (TiO), and 81 Da (TiO_2). Peaks related to Al (26 and 98 Da), SiCH (40 and 97 Da), AlSiH (56 and 96 Da) are related to the pigment coating formulation of the base paperboard consisting of kaolin clay, and are visible in the first stage wetted spectrum. Also the oxygen containing hydrocarbons produce stronger peaks at CHO (29.04 Da) and C_2H_3O (43.02 Da) in the first stage wetted channel. Stronger peaks at m/z = 41.04 Da, 43.06 Da, 55.06 Da, and the peaks between 91.06–165 are hydrocarbons found in the non-wetted channel and originate from the organic binder used in the pigment coating (Stepien et al. 2013).

The ToF-SIMS positive ion spectra were also recorded from areas surrounding the channel. No differences were detected between sample types, as one could expect, as the effect of the water in the first stage wetting is limited only to the channel area. In addition, the kaolin clay components are not visible for either samples in the outside areas. Small variations in Ti (46 and 48 Da) peak strengths were caused by slight sample-to-sample variations at the measurement spot.

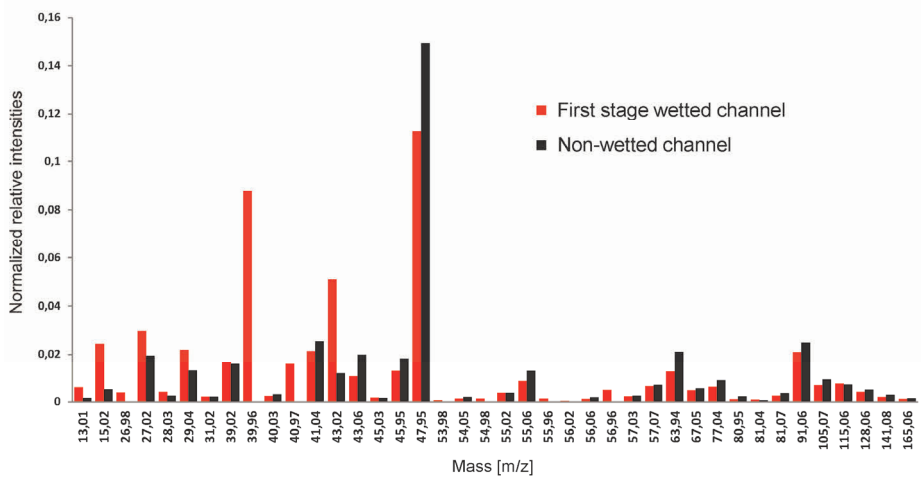

Figure 4.17 *ToF-SIMS normalized relative intensities for selected peaks in the channel area. (**Paper IV**)*

Chapter 5

Conclusion and Future Outlook

The present work utilized different coating and printing technologies to control electric and wetting performance of natural fibre-based substrates. These substrates are potential substitutes for fossil fuel-based plastic films in various value-added functional applications. A growing global population with a limited supply of both renewable and non-renewable raw materials sets an urgent demand for such sustainable transformation.

Water-based conductive ink PEDOT:PSS was applied in different amounts using successive flexography prints on various natural fibre-based substrates. Flexography allows large area conductive surfaces to be printed that can be combined with other printing technologies such as screen and inkjet printing for establishing cost-effective manufacturing of printed functionality such as solar cells. Addition of successive PEDOT:PSS layers on the substrate resulted in lower sheet resistance values, as expected. The TiO_2 nanoparticle coated paperboard has an additional degree of freedom with controlled wetting that can be used to control the ink setting on the surface. It was also shown that the surface superhydrophobicity remains under the dynamic printing process resulting in a reduced ink transfer and print density on such surface.

Paper surface is inherently rough and porous compared to smooth plastic film, which needs to be taken into account when targeting paper-based printed functionality. Conventional surface modification technologies used for graphical arts and packaging applications such as pigment coating, calendering, and dispersion barrier coating can be modified to meet the demands of printed functionality. Anionic and cationic polyelectrolytes are widely used in papermaking as dispersing agents in coating suspensions to prevent particle aggregation, and as additives to improve printability, e.g., in inkjet printing. Hence they are also present on the paper surface, as they usually fully cover the mineral pigment particle surfaces, and the concentration of polyelectrolytes can increase at the PEDOT:PSS - top coating interface. It was observed that on a cationic polyelectrolyte induces a conductivity increase that corresponded to 2-3 successive applications of PEDOT:PSS without polyelectrolytes. On the contrary, the anionic polyelectrolyte resulted in a lower conductivity.

Paper and paperboard are the most commonly used natural fibre-based substrates. However, they are limited by their opaque optical properties. Thus, they are not suitable candidates for display or solar cell applications that are currently realized on semi-transparent plastic and glass substrates. Recent advances in the fabrication of nanofibrillar cellulose (NFC) thin films have resulted in transparent films that avoid the opacity issue with traditional cellulose-based substrates. PEDOT:PSS was spin-coated on either drop cast or spin-coated NFC-glycerol (NFC-G) thin films. Glycerol was used as an anchor layer between the glass substrate and the NFC layer providing good adhesion. Improved conductivity was also observed, as glycerol is a secondary dopant for the PEDOT:PSS. A three-order-of-magnitude increase in the PEDOT:PSS conductivity was observed on the drop cast NFC-G substrates due to water and glycerol content in the substrate.

Finally, controlled and localized wetting of paperboard was achieved via a liquid flame spray (LFS) TiO_2 nanoparticle coating. Switchable wetting characteristics of such surfaces has been presented in the literature: ultraviolet radiation can be used to convert the initially superhydrophobic state to a highly hydrophilic one that can be reversed back to initial superhydrophobicity by a heat treatment. In this work, generation of permanent planar fluidic channels on such LFS TiO_2 nanoparticle coated paperboard was demonstrated. A simple water treatment after the UV irradiation was used to remove the nanoparticles from the wetted areas resulting in a permanent change in the wetting characteristics. Such planar fluidic channels can find applications, for example, in cost-effective, disposable point-of-care (POC) type diagnostic devices. An additional benefit of natural fibre substrates is easy disposability after use, e.g. by incineration, leaving no hazardous biological waste.

As a summary, the advances in printing science and technology have made it possible to embed functionality and intelligence practically everywhere. The Internet of Things (IoT) (Gershenfeld et al. 2004) is an emerging megatrend (see e.g. *Harvard Business Review* 2014) that is based on the integration of intelligent devices and sensors that analyse the environment and communicate with each other. For a widespread application of such devices, a number of device criteria have to be met: production methods must be cost-effective and the used materials flexible, suitable for roll-to-roll processing for smart structures and intelligent solutions that need to be integrated into packages, fabrics, and appliances. IoT has a large potential for significant cost savings: for example, in the western countries more than 100 kg food/capita is lost annually (Gustavsson et al. 2011). A large portion of the wasted food could be avoided

with better logistics and by using the feedback from biosensors in the packages stored in smart refrigerators.

Another example of such added functionality is intelligent medicine packaging with integrated medical drug uptake monitoring circuits that has been demonstrated by Stora Enso using RFID equipped medicine packages. Improvements in medical condition, healthcare, and life quality are in the centre of high-end diagnostics research and development. Lowered production costs, device miniaturization, and sufficient selectivity together with advances in wireless communications technology can revolutionize the future healthcare with significant cost saving potential. Furthermore, portable, close-to-patient, and cost-effective POC type diagnostic solutions can bring major improvements in life quality especially in developing countries, where seeking medical attention can be difficult due to long travel distances and limited laboratory resources. Quick remote healthcare with real-time monitoring possibility can also prevent the spreading of pandemics such as influenza or Ebola. Antibiotic resistance is another growing problem in the western countries that can be reduced by a correct use of antibiotics, i.e. not in the case of viral infections which is often the case nowadays due to lack of proper and quick diagnostics.

There is an increased demand for high production volumes of smart packages and disposable diagnostic devices. However, for a wide scale integration of such systems the single device needs to be very cost-effective, which can be achieved in roll-to-roll processes. At the same time, there is a real concern about the environmental load these solutions may cause. Therefore, research with sustainable, biodegradable, recyclable, and renewable natural fibre-based materials is in a key position to bring both ecologically and economically sustainable alternatives for replacing the existing non-renewable solutions. The forest industry sector has positioned itself well to meet these future demands.

References

Agarwal M, Lvov YM, Varahramyan K (2006), Conductive wood microfibres for smart paper through layer-by-layer nanocoating, *Nanotechnology*, 17, 5319.

Agarwal M, Xing Q, Shim BS, Kotov N, Varahramyan K, Lvov Y (2009), Conductive paper from lignocellulose wood microfibers coated with a nanocomposite of carbon nanotubes and conductive polymers, *Nanotechnology*, doi:10.1088/0957-4484/20/21/215602.

Alén R (2007), Papermaking Chemistry in Papermaking Science and Technology, 2nd ed. *Fapet Oy*, Helsinki (FI).

Aliahmad N, Agarwal M, Shrestha S, Varahramyan K (2013), Paper-based lithium-ion batteries using carbon nanotube-coated wood microfibers, *IEEE Trans Nanotechnol*, 12, 408–412.

Amin Y, Chen Q, Zheng LR, Tenhunen H (2012), Design and fabrication of wideband Archimedean spiral antenna based ultra-low cost\green modules for RFID sensing and wireless applications, *Prog Electromagn Res*, 130, 241.

Andersson P, Nilsson D, Svensson P-O, Chen M, Malmström A, Remonen T, Kugler T, Berggren M (2002), Active matrix displays based on all-organic electrochemical smart pixels printed on paper, *Adv Mater*, 14, 1460-1464.

Andersson P, Forchheimer R, Tehrani P, Berggren M (2007), Printable all-organic electrochromic active-matrix displays, *Adv Funct Mater*, 17, 3074.

Arena A, Donato N, Saitta G, Bonavita A, Risso G, Neri G (2010), Flexible ethanol sensors on glossy paper substrates operating at room temperature, *Sensors Actuators B Chem* 145, 488.

Arias AC, Ready SE, Lujan R, Wong WS, Paul KE, Salleo A, Chabinyc ML, Apte R, Street RA (2004), All jet-printed polymer thin-film transistor active-matrix backplanes, *Appl Phys Lett*, 85, 3304-3306.

Asadpoordarvish A, Sandström A, Larsen C, Bollström R, Toivakka M, Österbacka R, Edman L (2015), Light-emitting paper, *Adv Funct Mater*, 25, 3238-3245.

Bao Z (2000), Materials and fabrication needs for low-cost organic transistors circuits, *Adv Mater*, 12, 227-230.

Barr MC, Rowehl JA, Lunt RR, Xu J, Wang A, Boyce CM, Im SG, Bulovic V, Gleason KK (2011), Direct monolithic integration of organic photovoltaic circuits on unmodified paper, *Adv Mater*, 23, 3500.

Berggren M, Nilsson D, Robinson ND (2007), Organic materials for printed electronics. *Nature Materials*, 6, 3-5.

Biederman H (2004), Plasma polymer films, *Imperial College Press*, London (UK).

Björklund RB, Lundström I, Some properties of polypyrrole-paper composites (1984), *J Electron Mater*, 13, 211.

Bollström R, Määttänen A, Tobjörk D, Ihalainen P, Kaihovirta N, Österbacka R, Peltonen J, Toivakka M (2009), A multilayer coated fiber-based substrate suitable for printed functionality, *Org Electron*, 10, 1020-1023.

Bollström R, Tuominen M, Määttänen A, Peltonen J, Toivakka M (2012), Top layer coatability on barrier coatings, *Prog Org Coat*, 73, 26-32.

Caputo G, Nobile C, Kipp T, Blasi L, Grillo V, Carlino E, Manna L, Cingolani R, Cozzoli PD, Athanassiou A (2008), Reversible wettability changes in colloidal TiO_2 nanorod thin-film coatings under selective UV laser irradiation, *J Phys Chem C*, 112, 701-714.

Cassie ABD, Baxter S (1944), Wettability of porous surfaces, *Trans Faraday Soc*, 40, 546-551.

Cernakova L, Stahel P, Kovacik C, Johansson K, Cernak M (2006), Low cost high speed plasma treatment of paper surface, *Advanced Coating Fundamental Symposium Proceedings*, *TAPPI*, Turku (FI).

Courbat J, Kim YB, Briand D, de Rooi NF (2011), Inkjet printing on paper for the realization of humidity and temperature sensors, *Proceedings of 16th International SolidState Sensors, Actuators and Microsystems Conference 2011, TRANSDUCERS*, 13561359, Beijing, China.

Cui Z (2016), Printed electronics: Materials, Technologies and Applications, *John Wiley & Sons* Singapore Pte. Ltd., 2016.

Dalton JS, Preston JS, Heard PJ, Allen GC, Elton N, Husband JC (2002), Investigation into the distribution of ink components throughout printed coating paper – part 2: Utilizing XPS and SIMS, *Colloids Surf A*, 205, 199-213.

Dana SS, Liehr M, Anderle M, Rubloff GW (1992), Kinetics of nucleation and growth of Si on SiO_2 in very low pressure SiH_4 chemical vapor deposition, *Appl Phys Lett*, 61, 3035.

Das R, Zervos P (2012), Inorganic and composite printed electronics 2012-2012, IDTechEx.

Deegan RD, Bkajin O, Dupont TF, Huber G, Nagel SR, Witten TA (1997), Capillary flow as the cause of ring stains from dried liquid drops, *Nature*, 389(6653), 827-829.

Denneulin A, Blayo A, Bras J, Neuman C (2008), PEDOT:PSS coating on specialty papers: process optimization and effects of surface properties on electrical performances, *Prog Org Coat*, 63, 87.

Dufresne A (2013), Nanocellulose: a new ageless bionanomaterial, *Mater Today* 16, 220-227.

Dungchai W, Chailapakul O, Henry CS (2009), Electrochemical detection for paper-based microfluidics, *Anal Chem*, 81, 5821.

Elschner A, Kirchmayer S, Lovenich W, Merker U, Reuter K (2010), PEDOT: Principles and applications of an intrinsically conductive polymer, *CRC Press*, Boca Raton (FL), USA.

Eveleigh DE (1987), Cellulase: A perspective, *Philos Trans R Soc A,* 321, 435-447.

Fabretto M, Hall C, Vaithianathan T, Innis PC, Mazurkiewicz J, Wallace GG, Murphy P (2008), The mechanism of conductivity enhancement in poly(3,4ethylenedioxythiophene)–poly(styrenesulfonic) acid using linear-diol additives: its effect on electrochromic performance, *Thin Solid Films*, 516 7828-7835.

Fobel R, Kirby AE, Ng AHC, Farnood RR, Wheeler AR (2014), Paper microfluidics goes digital, *Adv Mater*, 26, 2838-2843.

Friedel B, Keivanidis PE, Brenner TJ, Abrusci A, McNeill CR, Friend RH, Greenham NC (2009), Effects of layer thickness and annealing of PEDOT:PSS layers in organic photodetectors, *Macromolecules*, 42, 6731-6747.

Friedel B, Brenner TJK, McNeill CR, Steiner U, Greenham NC (2011), Influence of solution heating on properties of PEDOT:PSS colloidal solutions and impact on the device performance of polymer solar cells, *Org Electron*, 12, 1736-1745.

Friedman A (2008), Plasma Chemistry, *Cambridge University Press*, New York (2008).

Fujishima A, Rao TN, Tryk DA (2000), Titanium dioxide photocatalysis, *J Photochem Photobiol C*, 1, 1-21.

Fukuzumi H, Saito T, Iwata T, Kumamoto Y, Isogai A (2009), Transparent and high gas barrier films of cellulose nanofibers prepared by TEMPO-mediated oxidation, *Biomacromolecules*, 10, 162–165.

Gershenfeld N, Krikorian R, Cohen D (2004), The internet of things, *Sci Am*, October Issue, 76–81.

Green JE, in Bunshah RF (Editor) (1994), Handbook of Deposition Technologies for Films and Coatings, 2nd Edition, *Noyes Publications*, Park Ridge, NJ, Ch 13, p 681.

Gross KA, Tikkanen J, Keskinen J, Pitkänen V, Eerola M, Siikamäki R, Rajala M (1999), Liquid flame spraying for glass coloring, *J Therm Spray Technol*, 8, 583-589.

Gunawan C, Teoh WY, Marquis CP, Lifia J, Amal R (2009), Reversible antimicrobial photoswitching in nanosilver, *Small*, 5, 341-344.

Gustavsson J, Cederberg C, Sonesson U, van Otterdijk R, Meybeck A (2011), Global Food Losses and Food Waste, *Food and Agriculture Organization of the United Nations (FAO) report*, Rome.

Hamedi MM, Campbell VE, Rothemund P, Güder F, Christodouleas DC, Bloch J-F, Whitesides GM (2016), Electrically activated paper actuators, *Adv Funct Mater*, 26, 2446-2453.

Harvard Business Review, The Internet of Everything, Issue November, 2014.

He J, Nuzzo RG, Rogers JA (2015), Assembly techniques for flexible and stretchable electronics, *Proc IEEE*, 103 (4), 619-632.

Howden RM, McVaya ED, Gleason KK (2013), oCVD poly(3,4ethylenedioxy-thiophene) conductivity and lifetime enhancement via acid rinse dopant exchange. *J Mater Chem A*, 1, 1334–1340.

Hu L, Zheng G, Yao J, Liu N, Weil B, Eskilsson M, Karabulut E, Ruan Z, Fan S, Bloking JT, McGehee MD, Wågberg L, Cui Y (2013), Transparent and conductive paper from nanocellulose fibers, *Energy Environ Sci*, 6, 513–518.

Huang B, Kang GJ, Ni Y, (2006), Preparation of conductive paper by in-situ polymerization of pyrrole in a pulp fibre system, *Pulp Pap Can*, 107, 38.

Hübler A, Trnovec B, Zillger T, Ali M, Wetzold M, Mingebach M, Wagenpfahl A, Deibel C, Dyakonov A (2011), Printed paper photovoltaic cells, *Adv Energy Mater*, 13, 1018.

Ihalainen P, Määttänen A, Järnström J, Tobjörk D, Österbacka R, Peltonen J (2012), Influence of surface properties of coated papers on printed electronics, *Ind Chem Eng Res,* 51, 6025.

Irimia-Vladu M, Głowacki ED, Voss G, Bauer S, Sariciftci NS (2012), Green and biodegradable electronics, *Mater Today*, 15, 340–346.

Izdebska J, Thomas S (Editors) (2016), Printing on polymers: fundamentals and applications, *Elsevier Inc*., Waltham (MA, USA), Chapters 4 and 5, 57-85.

Jaeger RC (2002), Introduction to Microelectronic Fabrication (2nd ed.), *Prentice Hall*, New Jersey (USA), 81–88.

Jang J, Ryu SK (2006), Physical property and electrical conductivity of electroless Ag-plated carbon fiber-reinforced paper, *J Mater Process Technol*, 180, 66.

Jariwala D, Sangwan VK, Lauhon LJ, Marks TJ, Hersam MC (2013), Carbon nanomaterials for electronics, optoelectronics, photovoltaics, and sensing, *Chem Soc Rev*, 42(7), 2824-2860.

Jonas F, Krafft W (1990), New polythiophene dispersions, their preparation and their use, *European Patent* EP0440957B1 (Bayer AG).

Keskinen H, Mäkelä JM, Aromaa M, Keskinen J, Areva S, Teixeira CV, Rosenholm J, Pore V, Ritala M, Leskelä M, Raulio M, Salkinoja-Salonen MS, Levänen E, Mäntylä T (2006), Titania and titania-silver nanoparticle deposits made by liquid flame spray and their functionality as photocatalyst for organic- and biofilm removal, *Catal Lett*, 111, 127–132.

Khan S, Lorenzelli L, Dahiya RS (2015), Technologies for printing sensors and electronics over large flexible subtrates: A review, *IEEE Sens J*, 15(6), 3164-3185.

Kim YH, Sachse C, Machala ML, May C, Müller-Meskamp L, Leo K (2011), Highly conductive PEDOT:PSS electrode with optimized solvent and thermal post-treatment for ITO-free organic solar cells, *Adv Funct Mater*, 21, 1076–1081.

Kipphan H (2001), Handbook of Print Media: Technologies and Production Methods, *Springer Science & Business Media, Springer-Verlag*, Berlin (DE).

Koivula H, Kamal Alm H, Toivakka M (2011), Temperature and moisture effects on wetting of calcite surfaces by offset ink constituents, *Colloids Surf A*, 390, 105.

Kumar V, Bollström R, Yang A, Chen Q, Chen G, Salminen P, Bousfield D, Toivakka M (2014), Comparison of nano-and microfibrillated cellulose films, *Cellulose*, 21, 3443–3456.

Kuusipalo J (2008), Paper and Paperboard Converting, Vol 12, *Fapet Oy*, Helsinki (FI).

Kuusipalo J, Savolainen A, Adhesion phenomena in (co)extrusion coating of paper and paperboard (1997), *J Adhes Sci Technol*, 11, 1119-1135.

Laakso P, Ruotsalainen S, Halonen E, Kemppinen A, Mäntysalo M (2009), Sintering of printed nanoparticle structures using laser treatment, *Proceedings of the 5th international WLT-Conference on lasers in manufacturing,* June 15-18, Munich, DE, 527-532.

Li G, Shrotriya V, Huang J, Yao Y, Moriarty T, Emery K, Yang Y (2005) High-efficiency solution processable polymer photovoltaic cells by self-organization of polymer blends, Nature Materials **4**, 864 – 868.

Liu J, Korpinen R, Mikkonen KS, Willför S, Xu C (2014), Nanofibrillated cellulose originated from birch sawdust after sequential extractions: a promising polymeric material from waste to films, *Cellulose*, 21, 2587–2598.

Liu XY, O'Brien M, Mwangi M, Li XI, Whitesides GM (2011), Paper-based piezoresistive MEMS force sensor, *Proceedings of 2011 IEEE 24th International Conference on Micro Electro Mechanical Systems (MEMS)*, 133–136, Cancun, Mexico.

Logothetidis S (Editor) (2014), Handbook of Flexible Organic Electronics. Materials, Manufacturing and Applications (1st Ed.), *Woodhead Publishing*, Cambridge, UK.

Löwenich W (2014), PEDOT – properties and applications, *Polym Sci Ser C*, 56, 135.

Magdassi S (Editor) (2009), The chemistry of inkjet inks, *World Scientific Publishing Company Co. Pte. Ltd.*, Singapore.

Martinez AW, Phillips ST, Whitesides GM (2008), Three-dimensional microfluidic devices fabricated in layered paper and tape, *Proc Nat Acad Sci*, 105, 19606-19611.

Martinez AW, Phillips ST, Whitesides GM, Carrilho E (2010), Diagnostics for the developing world: Microfluidic paper-based analytical devices, *Anal Chem*, 82, 3-10.

Mattana G, Briand D (2016), Recent advances in printed sensors on foil, *Materials Today*, 19(2), 89-99.

McCarthy JE, Hanley CA, Brennan LJ, Lambertini VG, Gun'ko YK (2014), Fabrication of highly transparent and conducting PEDOT:PSS films using a formic acid treatment, *J Mater Chem C*, 2, 764–770.

McCulloch I, Heeney M, Bailey C, Genevicius K, MacDonald I, Shkunov M, Sparrowe D, Tierney S, Wagner R, Zhang W,Chabinyc ML, Kline RJ, McGehee MD, Toney MF (2006), Liquid-crystalline semiconducting polymers with high charge-carrier mobility, *Nature Materials*, 5, 328 - 333.

Mochizuki Y, Horii T, Okuzaki H (2012), Effect of pH on structure and conductivity of PEDOT/PSS, *Trans Mater Res Soc Jpn*, 37, 307.

Montibon E, Lestelius M, Järnström L (2010), Electroconductive paper prepared by coating with blends of poly(3,4-ethylenedioxythiophene)/poly(4-styrenesulfonate) and organic solvents, *J Appl Polym Sci*, 117, 3524.

Mäkelä JM, Keskinen H, Forsblom T, Keskinen J (2004), Generation of metal and metal oxide nanoparticles by liquid flame spray process, *J Mater Sci*, 39, 2783–2788.

Mäkelä JM, Hellsten S, Silvonen J, Vippola M, Levänen E, Mäntylä T, (2006), Collection of liquid flame spray generated TiO_2 nanoparticles on stainless steel surface, *Mater Lett*, 60, 530-534.

Mäkelä JM, Aromaa M, Teisala H, Tuominen M, Stepien M, Saarinen JJ, Toivakka M, Kuusipalo J (2011), Nanoparticle deposition from liquid flame spray onto moving roll-to-roll paperboard material, *Aerosol Sci Technol*, 45, 817-827.

Mäkelä T, Jussila S, Vilkman M, Kosonen H, Korhonen R (2003), Roll-to-roll method for producing polyaniline patterns on paper, *Synth Met*, 135–136, 41.

Määttänen A, Vanamo U, Ihalainen P, Pulkkinen P, Tenhu H, Bobacka J, Peltonen J (2013), A low-cost paper-based inkjet-printed platform for electrochemical analyses, *Sensors Actuators B Chem*, 177, 153.

Möller M, Leyland N, Copeland G, Cassidy M (2010), Self-powered electrochromic display as an example for integrated modules in printed electronics applications, *Eur Phys J Appl Phys*, 51, 33205.

Nardes AM (2007), On the conductivity of PEDOT:PSS thin films. *PhD Thesis*, Technische Universiteit Eindhoven (The Netherlands).

Nelo M (2016), Inks based on inorganic nanomaterials for printed electronics applications. *PhD Thesis*, University of Oulu (Finland).

Nie Z, Nijhuis CA, Gong J, Chen X, Kumachev A, Martinez AW, Narovlyansky M, Whitesides GM (2010), Electrochemical sensing in paper-based microfluidic devices, *Lab Chip*, 10, 477.

Ouyang J, Xua Q, Chu C-W, Yang Y, Gang Lib, Joseph Shinar (2004), On the mechanism of conductivity enhancement in poly(3,4-ethylenedioxythiophene):poly(styrene sulfonate) film through solvent treatment, *Polymer*, 45, 8443–8450.

Ouyang J, Chu C, Chen F, Xu Q, Yang Y (2005), High-conductivity poly(3,4ethylene-dioxythiophene): poly(styrenesulfonate) film and its application in polymer opto-electronic devices, *Adv Funct Mater*, 15, 203–208.

Padinger F, Rittberger RS, Sariciftci NS (2003), Effects of postproduction treatment on plastic solar cells, *Adv Funct Mater*, 13, 85-88.

Paltakari J (2009), Pigment Coating and Surface Sizing of Paper, 2nd edition, *Fapet Oy*, Helsinki (FI).

Pelton R (2009), Bioactive paper provides a low-cost platform for diagnostics, *Trends Anal Chem*, 28, 925–942.

Peng CQ, Thio YS, Gerhardt RA (2008), Conductive paper fabricated by layer-by-layer assembly of polyelectrolytes and ITO nanoparticles, *Nanotechnology*, 19, 505603.

Perelaer J, Smith PJ, Mager D, Soltman D, Volkman SK, Subramanian V, Korvink JG, Schubert US (2010), Printed electronics: the challenges involved in printing devices, interconnects, and contacts based on inorganic materials, *J Mater Chem*, 20, 8446-8453.

Perelaer J, Schubert US (2013), Novel approaches for low temperature sintering of inkjet-printed inorganic nanoparticles for roll-to-roll (R2R) applications, *J Mater Res*, 28(4), 564–573,

Perepichka IF (Editor), Perepichka DF (Edditor) (2009), Handbook of thiophene-based materials, Applications in organic electronics and photonics, *John Wiley & Sons*, UK.

Pykönen M, Sundquist H, Järnström J, Kaukoniemi O-V, Tuominen M, Lahti J, Peltonen J, Fardim P, Toivakka M (2008), Effects of atmospheric plasma activationon surface properties of pigment coated and surface-sized papers, *Appl Surf Sci*, 255, 3217-3229.

Qian X, Song H, Wang L (2006), Conductive paper manufactured with the composite of polyaniline/pulp fiber by in situ polymerization, *Proc. from the 3rd International Symposium on Emerging Technologies of Pulp and Papermaking, Guangzhou, China*, 434.

Ritala M, Leskelä M, in Nalwa HS (Editor) (2001), Handbook of Thin Film Materials, *Academic Press*, San Diego (USA), Vol 1, Ch 2, 103.

Saarinen JJ, Valtakari D, Haapanen J, Salminen T, Mäkelä JM, Uozumi J (2014), Surface-enhanced Raman scattering active substrates by liquid flame spray deposited and inkjet printed silver nanoparticles, *Opt Rev*, 21, 339-344.

Saarinen JJ, Valtakari D, Sandén S, Haapanen J, Salminen T, Mäkelä JM, Uozumi J (2017), Roll-to-roll manufacturing of disposable surface-enhanced Raman scattering (SERS) sensors on paper based substrates, *Nord Pulp Pap Res J*, 32, 222-228.

Salajkova M, Valentini L, Zhou Q, Berglung LA (2013), Tough and conductive nanopaper structures based on cellulose nanofibrils and carbon nanotubes, *Compos Sci Technol*, 87, 103–110.

Salas C, Nypelö T, Rodriguez-Abreu C, Carrillo C, Rojas OJ (2014), Nanocellulose properties and applications in colloids and interfaces. *Curr Opin Colloid Interface Sci*, 19, 383–396.

Sarfraz J, Määttänen A, Ihalainen P, Keppeler M, Lindén M, Peltonen J (2012), Printed copper acetate based H_2S sensor on paper substrate, *Sensors Actuators B Chem*, 173, 868-873.

Sauer HM, Daume D, Dörsam E (2015), Lubrication theory of ink hydrodynamics in the flexographic printing nip, *J Print Media Technol Res*, 4, 163-172.

Schneider J, Matsuoka M, Takeuchi M, Zhang J, Horiuchi Y, Anpo M, Bahnemann DW. Understanding TiO_2 photocatalysis: mechanisms and materials. Chemical Reviews, 114, pp. 9919-9986 (2014).

Sekine C, Tsubata Y, Yamada T, Kitano M, Doi S (2014), Recent progress of high performance polymer OLED and OPV materials for organic printed electronics, *Sci Tech Adv Mater*, 15(4), 034203.

Shinagawa S, Kumagai Y, Urabe K (1999), Conductive papers containing metallized polyester fibers for electromagnetic interference shielding, *J Porous Mater*, 6, 185.

Sneh O, Clark-Phelps RB, Londergan AR, Winkler JL, Seidel TE (2002), *Thin Solid Films*, 402/1-2, 248.

Siegel AC, Phillips ST, Wiley BJ, Whitesides GM (2009), Thin, lightweight, foldable thermochromic displays on paper, *Lab on Chip*, 9, 2775-2781.

Søndergaard RR, Hösel M, Krebs FC (2013), Roll-to-roll fabrication of large area functional organic materials, *J Polym Sci Part B Polym Phys*, 51, 16-34.

Songok J, Tuominen M, Teisala H, Haapanen J, Mäkelä J, Kuusipalo J, Toivakka M (2014), Paper-based microfluidics: Fabrication technique and dynamics of capillary driven surface flow, *ACS Appl Mater Interfaces*, 6, 20060-20066.

Stepien M, Saarinen JJ, Teisala H, Tuominen M, Aromaa M, Kuusipalo J, Mäkelä JM, Toivakka M (2011), Adjustable wettability of paperboard by liquid flame spray nanoparticle deposition, *Appl Surf Sci*, 257, 1911-1917.

Stepien M, Saarinen JJ, Teisala H, Tuominen M, Aromaa M, Kuusipalo J, Mäkelä JM, Toivakka M (2012), Surface chemical analysis of photocatalytic wettability conversion of TiO_2 nanoparticle coating, *Surf Coat Technol*, 208, 73–79.

Stepien M, Saarinen JJ, Teisala H, Tuominen M, Aromaa M, Haapanen J, Kuusipalo J, Mäkelä JM, Toivakka M (2013), ToF-SIMS analysis of UV-switchable TiO_2 nanoparticle-coated paper surface, *Langmuir*, 29, 3780–3790.

Teisala H, Tuominen M, Stepien M, Haapanen J, Mäkelä JM, Saarinen JJ, Toivakka M, Kuusipalo J (2013), Wettability conversion on the liquid flame spray generated superhydrophobic TiO_2 nanoparticle coating on paper and board by photocatalytic decomposition of spontaneously accumulated carbonaceous overlayer, *Cellulose*, 20, 391-408.

Tekin E, Holder E, Marin V, de Gans J-P, Schubert US (2005), Ink-jet printing of luminescent ruthenium- and iridium-containing polymers for applications in light-emitting devices, *Macromol Rapid Commun*, 26, 293–297.

Tendero C, Tixier C, Tristant P, Desmaison J, Leprince P (2006), Atmospheric pressure plasmas: A review, *Spectrochim Acta B*, 61, 2-30.

Tobjörk D, Kaihovirta NJ, Mäkelä T, Pettersson FS, Österbacka R (2008), All-printed low-voltage organic transistors, *Org Electron*, 9, 931-935.

Tobjörk D, Österbacka R (2011), Paper electronics, *Adv Mater*, 23, 1935.

Torvinen K, Sievänen J, Hjelt T, Hellén E (2012), Smooth and flexible filler nanocellulose composite structure for printed electronics applications, *Cellulose,* 19, 821–829.

Trnovek B, Stanel M, Hahn U, Hübler AC, Kempa H, Sangl R, Foster M (2009), Coated paper for printed electronics, *Prof Papermak*, 6, 48.

Ullman A (1995), Characterization of Organic Thin Films. *Butterworth-Heinemann*, Stoneham (MA, USA).

Unander T, Nilsson H-E (2009), Characterization of printed moisture sensors in packaging surveillance applications, *IEEE Sensors J*, 9, 922.

Valtakari D, Bollström R, Toivakka M, Saarinen JJ (2015) Influence of anionic and cationic polyelectrolytes on the conductivity and morphology of poly(3,4-ethylene-dioxythiophene): poly(styrenesulfonate) films, *Thin Solid Films*, 590, 170–176.

Valtakari D, Stepien M, Haapanen J, Teisala H, Tuominen M, Kuusipalo M, Mäkelä JM, Toivakka M, Saarinen JJ (2016), Planar fluidic channels on TiO_2 nanoparticle coated paperboard, *Nord Pulp Pap Res J*, 31, 232–238.

van Oss CJ (2006), Interfacial Forces in Aqueous Media (2nd ed.), *Taylor & Francis*, Boca Raton (USA).

Vosgueritchian M, Lipomi DJ, Bao Z (2012), Highly conductive and transparent PEDOT:PSS films with a fluorosurfactant for stretchable and flexible transparent electrodes, *Adv Funct Mater*, 22, 421–428.

Vähä-Nissi M, Kimpimäki T, Kuusipalo J, Savolainen A (1997), Adhesion in extrusion coating of dispersion coated paper/paperboard, *TAPPI Polymers, Laminations & Coatings Conference*, Toronto, Canada, 559-566.

Wang HL, Toppare L, Fernandez JE (1990), Conducting polymer blends: polythiophene and polypyrrole blends with polystyrene and poly(bisphenol A carbonate), *Macromolecules*, 23 (4), 1053–1059.

Wenzel RW (1936), Resistance of solid surfaces to wetting by water, *Ind Eng Chem*, 28, 988–994.

Wistrand I, Lingström R, Wågberg L (2007), Preparation of electrically conducting cellulose fibres utilizing polyelectrolyte multilayers of poly(3,4-ethylenedioxythio-phene): poly(styrene sulphonate) and poly(allyl amine), *Eur Polym J*, 43, 4075.

Wong JE, Rehfeldt F, Hänni P, Tanaka M, Klitzing Rv (2004), Swelling behaviour of polyelectrolyte multilayers in saturated water vapor, *Macromolecules*, 37, 7285-7289.

Xue J, Song F, Yin X, Wang X, Wang Y (2015), Let it shine: a transparent and photo-luminescent foldable nanocellulose/quantum dot paper, *ACS Appl Mater Interfaces*, 7, 10076–10079.

Yan H, Jo T, Okuzaki H (2011), Potential application of highly conductive and transparent poly(3,4-ethylenedioxythiophene)/poly(4-styrenesulfonate) thin films to touch screen as a replacement for indium tin oxide electrodes, *Polym J*, 43, 662–665.

Yang L, Rida R, Vyas M, Tentzeris MM (2007), RFID tag and RF structures on a paper substrate using inkjet-printing technology, *IEEE Trans Microwave Theory Tech*, 55, 2894.

Yoshiki T, Shino S, Kobayashi K (2007), Process for preparing conductive material (導電性材料の製造方法), *Patent* WO 2007148773 A1 (Mitsubishi Paper Mills Ltd.).

Young T (1805), An essay on the cohesion of fluids, *Philos T R Soc Lond*, 95, 65–87.

Zheng Z, McDonald J, Khillan R, Su Y, Shutava T, Grozditz G, Lvov YM (2006), Layer-by-layer nanocoating of lignocellulose fibers for enhanced paper properties, J Nanosci Nanotechnol, 6, 624.

Zheng G, Cui Y, Karabulut E, Wågberg L, Zhu H, Hu L (2013), Nanostructured paper for flexible energy and electronic devices, *MRS Bull*, 38, 320–325.

Zhu H, Xiao Z, Liu D, Li Y, Wadock NJ, Fang Z, Huang J, Ku L (2013), Biodegradable transparent substrates for flexible organic light-emitting diodes, Energy Environ Sci, 6, 2105–2111.

ISBN 978-952-12-3652-5